Estuarine, Coastal and Shelf Science 323 (2025) 109424

Contents lists available at ScienceDirect

Estuarine, Coastal and Shelf Science

journal homepage: www.elsevier.com/locate/ecss

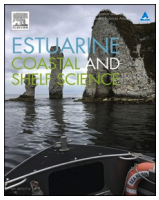

High-energy systems are underrepresented in global porewater studies of sandy beach aquifers

Gudrun Massmann [a,b,*], Janek Greskowiak [a,b], Julius Degenhardt [b], Bert Engelen [b], Moritz Holtappels [c], Rena Meyer [a,b], Mike Müller-Petke [d], Nils Moosdorf [e], Jutta Niggemann [b], Katharina Pahnke [b], Vincent Post [f], Anja Reckhardt [b], Kai Schwalfenberg [b], Stephan Seibert [a,b], Hannelore Waska [b], Christian Winter [g]

[a] Institute of Biology and Environmental Science (IBU), School of Mathematics and Science, Carl von Ossietzky Universität Oldenburg, Oldenburg, Germany
[b] Institute for Chemistry and Biology of the Marine Environment (ICBM), School of Mathematics and Science, Carl von Ossietzky Universität Oldenburg, Oldenburg, Germany
[c] Alfred-Wegener-Institute, Helmholtz Centre for Polar and Marine Research, Bremerhaven, Germany
[d] Leibniz-Institute for Applied Geophysics, Hannover, Germany
[e] Leibniz Zentrum für Marine Tropenforschung, Bremen, Germany
[f] Edinsi groundwater, Nederhorst den Berg, the Netherlands
[g] Institute for Geosciences, University of Kiel, Germany

ARTICLE INFO

Keywords:
Coastal aquifer
Subterranean estuary
Submarine groundwater discharge
Coastal ecology
Elemental cycles
Groundwater
Land-sea interface

ABSTRACT

Aquifers beneath sandy beaches act as land-ocean conduits for groundwater and are active biogeochemical reactors modifying chemical fluxes across the land-sea interface. Subterranean estuaries of high-energy beaches with large tidal and wave amplitudes could be particularly reactive due to the exchange of large seawater volumes and transport of marine derived constituents deep into the subsurface. In this study, we first present a new classification for coastal energy regimes as a function of mean tidal range and mean significant wave height and define the term "high-energy". We establish a global distribution map of coastal energy regimes and classify porewater study sites in sandy beach aquifers related to their prevalent energy regime. Despite their extensive contribution to the global shoreline, the porewater biogeochemistry of high-energy environments is largely unknown. Through a summary of the few existing porewater studies at high-energy beaches we reveal patterns in morphology, hydrology, and biogeochemistry, describe promising research strategies, and highlight future research avenues in these challenging environments.

1. Introduction

Sandy beaches are common features of global coastlines, covering about a third of ice-free shores (Luijendijk et al., 2018). They are dynamic environments where sea and land meet and the energy of the oceanic forces of wind, waves and tides dissipates and drives sediment transport and morphodynamics (McLachlan and Defeo, 2018). Sandy beaches host coastal ecosystems that are intrinsically valuable but also provide important ecosystem services (e.g. storm buffering, nutrient cycling, habitat provision) and are of economic and cultural importance (Nel et al., 2014). McLachlan and Turner (1994) described exposed beach ecosystems as the most dynamic and most hostile of all marine environments, yet bristling with micro- and macroscopic life (McLachlan and Defeo, 2018).

The subsurface beneath beaches is referred to as beach aquifer (Geng et al., 2021b) or subterranean estuary (STE, Moore (1999), for a discussion on the terminology used see also Duque et al. (2020). In these, inland aquifers connect with the sea and meteoric freshwater mixes with recirculating seawater, both undergoing biogeochemical changes before discharging to the coastal ocean. STEs are important biogeochemical reactors that alter elemental speciation and net fluxes to the sea (e.g. Moore, 1999; Charette and Sholkovitz, 2006; Anschutz et al., 2009; Reckhardt et al., 2015; Linkhorst et al., 2017; Wilson et al., 2024). Water discharging from STEs is termed submarine groundwater discharge

* Corresponding author. Institute of Biology and Environmental Science (IBU), School of Mathematics and Science, Carl von Ossietzky Universität Oldenburg, Oldenburg, Germany.
E-mail address: gudrun.massmann@uni-oldenburg.de (G. Massmann).

https://doi.org/10.1016/j.ecss.2025.109424
Received 23 August 2024; Received in revised form 22 April 2025; Accepted 29 June 2025
Available online 30 June 2025

(SGD, e.g. Michael et al., 2005; Robinson et al., 2007a). SGD has been recognised as a major input pathway for solutes to coastal waters that is affecting coastal elemental cycles and budgets, coastal surface water quality and coastal ecosystems (e.g. Santos et al., 2008; Moore, 2010; Lecher et al., 2016; Rodellas et al., 2015; Ehlert et al., 2016; Beck et al., 2017; Sawyer et al., 2016; Geng et al., 2021b; Moosdorf et al., 2021).

Coastal zones and sandy coasts in particular belong to the most densely populated and developed land areas worldwide (Luijendijk et al., 2018). Consequently, sandy beaches are threatened by extractive use, habitat modification and development, coastal squeeze and sea-level rise (Nel et al., 2014). Similarly, coastal groundwater is under considerable strain, with natural groundwater flow patterns being disrupted and freshwater resources often affected by overuse and contamination (Michael et al., 2017). According to review papers by Michael et al. (2017) and Robinson et al. (2018) a sound understanding on groundwater flow and solute transport and accompanying reactions at the land-sea transition zone is necessary in order to manage coastal groundwater resources properly.

The general perception of groundwater flow and transport in tidally influenced beach aquifers is the existence of a tide-induced saltwater circulation cell, often referred to as upper saline plume (USP) that is underlain by a freshwater discharge tube (FTD), itself underlain by the so-called saltwater wedge (Michael et al., 2005; Robinson et al., 2007b, Fig. 1, "stable" case). In a simple geological setting, fresh and saline groundwater discharge to the sea near the low water line (LWL). The occurrence, dimensions and shape of the USP depend on a number of hydrological parameters, such as hydraulic conductivity, terrestrial freshwater flux, tidal amplitude, wave heights, beach slope and aquifer depth (e.g. Evans and Wilson, 2016; Grünenbaum et al., 2020b). For example, spring and neap tidal cycles (Robinson et al., 2007a; Abarca

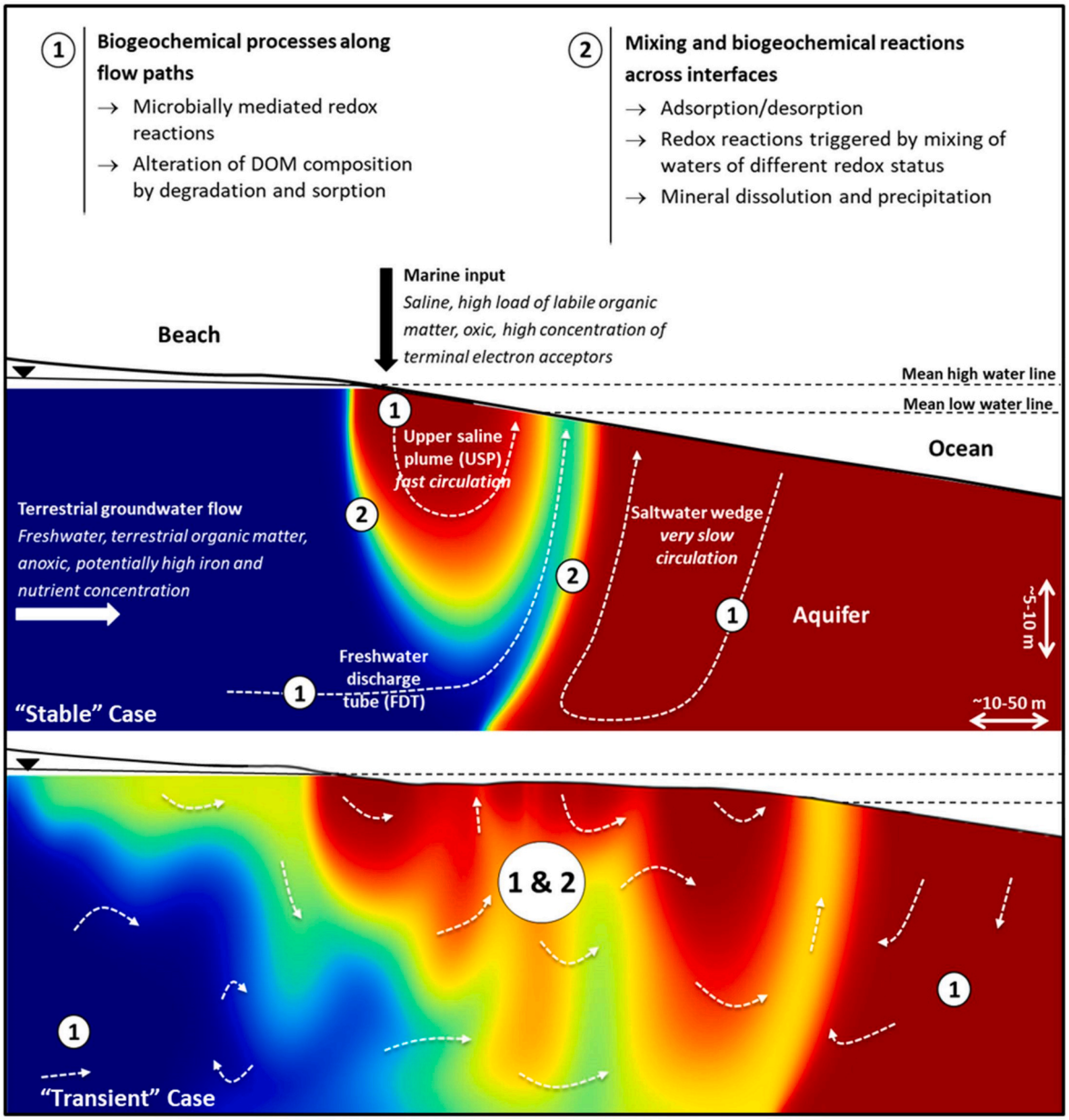

Fig. 1. Concept of the STE under tidal influence as a biogeochemical reactor with general features such as different water bodies, flow patterns and porewater salinities (colour scale from saltwater in red to freshwater in blue). Principle features of mixing seawater and terrestrial freshwater as well as major biogeochemical processes expected along flow paths (1) and at interfaces (2) are listed at the top. The "stable" case represents the state-of-the-art, whereas the "transient" case was proposed for high-energy beaches by Greskowiak and Massmann (2021), figure by Massmann et al. (2023). (For interpretation of the references to color in this figure legend, the reader is referred to the Web version of this article.)

et al., 2013; Heiss and Michael, 2014) and intensified wave conditions (Robinson et al., 2014) can lead to varying seawater circulation rates and thus dynamic shrinkage and expansion of the USP. In experiments and numerical modelling, instabilities and fingering flow occurred in STEs under certain hydraulic conditions, such as flat beach slopes (Greskowiak, 2014; Röper et al., 2015; Shen et al., 2019), but the process has so far not been observed in the field. Moreover, on top of the major physical stressors (waves, tides, density gradients, precipitation, evaporation and storm surges) that control groundwater flow and transport, geological heterogeneity may increase the complexity of the flow patterns in beach aquifers (Geng et al., 2021b). Considerable sediment transport capacities of the combined tidal and wave forcing continuously reshape high-energy beaches on very short time scales (Blossier et al., 2016, 2017). Consequently, Greskowiak and Massmann (2021) proposed that morphodynamics might affect groundwater flow and transport. In their generic numerical models, beach morphodynamics and regular storm-floods disrupted the classic salinity distribution and caused strong variability in beach groundwater flow and transport patterns. The resulting SGD was associated with topographic lows that frequently changed location, in turn causing movements of the salt- and freshwater interface. Fluctuating sediment transport and morphodynamics, key features of high-energy environments, therefore resulted in remarkably chaotic porewater flow patterns that deviated from the conventional, "stable" case (Greskowiak and Massmann, 2021, Fig. 1, "transient" case).

The hydrodynamic conditions in beaches subsequently exert a major control on rates and spatial distribution of biogeochemical processes in the STE (e.g. Charette and Sholkovitz, 2002; McAllister et al., 2015; Reckhardt et al., 2017). In most STEs, oxygen and marine dissolved organic matter (DOM) are supplied by infiltrating seawater (Beck et al., 2017; Massmann et al., 2023). From the landside, fresh groundwater entering the beach aquifer contains more aged terrestrial DOM (Waska et al., 2021) and is often anoxic. It can be enriched with inorganic nitrogen from anthropogenic contamination, a commonly limiting nutrient in ocean waters (Howarth and Marino, 2006), as well as reduced iron (Charette and Sholkovitz, 2002). As these very different porewater endmembers mix in beach aquifers, they result in pronounced physicochemical gradients (Moore, 1999; Greskowiak et al., 2023) that trigger biogeochemical processes. These are mainly related to redox reactions coupled to microbial organic matter (OM) degradation, and mineral dissolution/precipitation (e.g. Anwar et al., 2014; McAllister et al., 2015; Reckhardt et al., 2015; Kim et al., 2017; Kim et al., 2020). Some processes were shown to be mixing controlled and more intense at interfaces (Fig. 1, indicated by number 2) such as the formation of iron (III)-(hydr)oxide-coated sands in the STE (e.g. Grünenbaum et al., 2024), a phenomenon termed "iron curtain" by Charette and Sholkovitz (2002). The iron curtain has been proposed to act as a geochemical barrier for water constituents such as P and As (Moosdorf et al. (2021) and references therein) and DOM (Linkhorst et al., 2017; Sirois et al., 2018). Other biogeochemical processes progress along flowpaths in the different water bodies (i.e. USP, FDT and saltwater wedge, Fig. 1, indicated by number 1), for example mineralisation of OM following seawater infiltration (e.g. McAllister et al., 2015; Reckhardt et al., 2015; Charbonnier et al., 2016). Since biogeochemical processes are so closely associated with porewater flow patterns - which in turn are influenced by morphodynamics - they too likely differ on spatial and temporal scales between stable and transient systems. Recently, Massmann et al. (2023) proposed that the transient groundwater flow and transport typical for high-energy beaches (Greskowiak and Massmann, 2021) also affect the functioning of the biogeochemical reactor, as interfaces between water bodies are not position stable and flow paths irregular. Corroborating this suggestion by means of generic modelling, Greskowiak et al. (2023) indeed identified morphodynamics as the dominant factor controlling redox dynamics as compared to stormfloods, seasonal temperature and recharge rates.

As the main protagonists of the STE bioreactor, microbial communities are structured by the availability of substrates and electron acceptors (McAllister et al., 2015; McBeth et al., 2013; Degenhardt et al., 2021, 2021a, 2021b). A continuous electron acceptor and OM supply ensures that microbial activities in STEs and shallow beach sediments are high (Forehead et al., 2013; Hwang et al., 2005; Santos et al., 2008; Reckhardt et al., 2015; Beck et al., 2017). However, the understanding of biogeochemical processes controlling microbial life in STEs and associated microbial transformations is still limited (McAllister et al., 2015; Kim et al., 2017). As reviewed by Archana et al. (2021), only few studies so far targeted the STE and its characteristics as a unique microbial habitat. The potential consequences of a "transient" STE as proposed in Fig. 1 are unclear.

As outlined above, physical forcing, chemical gradients and biological processes are intrinsically linked in beach STEs. However, most STE knowledge, including - crucially - the state-of-the-art "stable" concept of flow, transport and biogeochemical reactions (Fig. 1), is derived from beach aquifers at rather sheltered sites. Contrastingly, it appears that only little data, especially regarding porewater biogeochemistry, is available from high-energy beaches with meso-to macrotidal ranges and/or high wave impact, although seawater recirculation through tide and wave pumping is considered a major driver of SGD hydrology (Santos et al., 2012). Moreover, despite being used in the STE literature, the term "high-energy" is not clearly defined. McLachlan et al. (2018) stated that accurate information on environmental conditions (i.e. particle size, tidal range and wave height) is necessary when studying beach ecology, but often not provided. The same is true for biogeochemical porewater studies in STEs, that often do not report comprehensively on the environmental site conditions.

Therefore, the aims of this paper are to first (i) present a simple definition of coastal beach energy regimes and (ii) provide a map on their global distribution, (iii) conduct a literature study to identify the distribution of beach aquifer porewater studies across the different energy regimes, (iv) briefly summarize findings from those conducted at high-energy beaches, to finally (v) discuss specific features, existing knowledge gaps and methodological difficulties encountered in high-energy studies.

2. Definition and global distribution of beach energy classes

Sandy coasts are shaped by the continuous interplay of morphology and sediments with waves, tides, currents and wind. Coastal energy regimes are classified depending on tidal range and mean significant wave heights (Mulhern et al., 2017). Hayes (1979) subdivided tidal ranges into microtidal (0–1 m), low-mesotidal (1–2 m), high-mesotidal (2–3.5 m), low macrotidal (3.5–5 m) and macrotidal (>5 m) conditions. Mean significant wave heights were further classified into low (<0.6 m), mean (0.6–1.5 m) and high (>1.5 m) wave energies, respectively. Hayes (1979) subsequently defined five different energy classes that he linked to barrier island shapes: Wave-dominated, mixed energy (wave-dominated), mixed energy (tide-dominated), tide dominated and strongly tide-dominated (high), emphasizing the respective force causing the energy (i.e. tide or waves).

We suggest combining wave and tidal classes in a different way to define the overall energy regime of a beach. Hayes' original work addressed the effects of tides and waves on the stability of barrier islands separately, as both drivers have opposing effects. Our new classification instead considers the combined effect of waves and tides on the hydraulic forcing within the STE. This acknowledges the fact that both higher wave and tidal energy enhance seawater circulation in STEs. Moreover, high-energy conditions are generally associated with coarser beach sediments with a high permeability, thereby reinforcing the effects of high waves and tides. Our new approach results in four distinct energy classes (low, lower moderate, upper moderate and high) as shown in Fig. 2. Instead of classes forming bands radiating away from the origin as in the Hayes classification, classes are separated by ellipses around the origin. Here, the boundaries on both the semi-minor axis

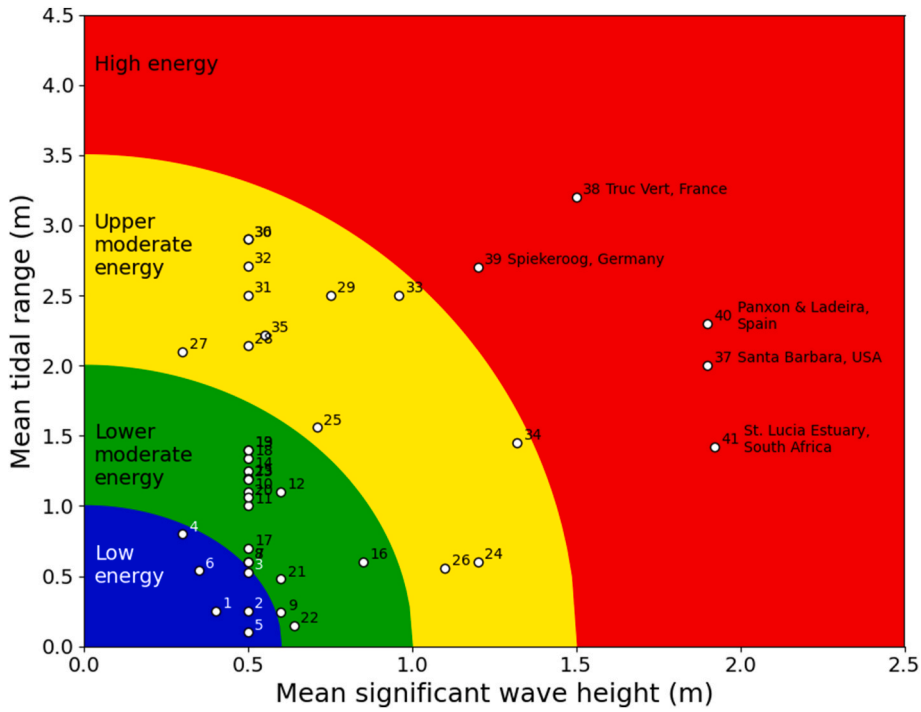

Fig. 2. Beach energy classes given as a function of mean tidal range and mean significant wave height. Blue denotes low energy, green lower moderate energy, yellow upper moderate and red high-energy conditions. Field sites of STE porewater studies (sampling depth >0.5 m) from sandy beaches reported in the literature are shown as circles, site numbers according to Table 1 and supplementary. Only high-energy sites that are briefly summarized in this paper are named. (For interpretation of the references to color in this figure legend, the reader is referred to the Web version of this article.)

(mean tidal range) and the semi-major axis (mean significant wave height) are adopted from Hayes (1979), with the only difference that we (i) separated the mean wave energy (0.6 m–1.5) into a lower mean and higher mean at a mean significant wave height of 1 m and (ii) joined the low macrotidal and macrotidal regime. As the limiting values for tide range and wave height for defining the energy classes were adopted from the Hayes classification for barrier island stability, their usefulness for inferring on characteristic flow and transport patterns in the STE is

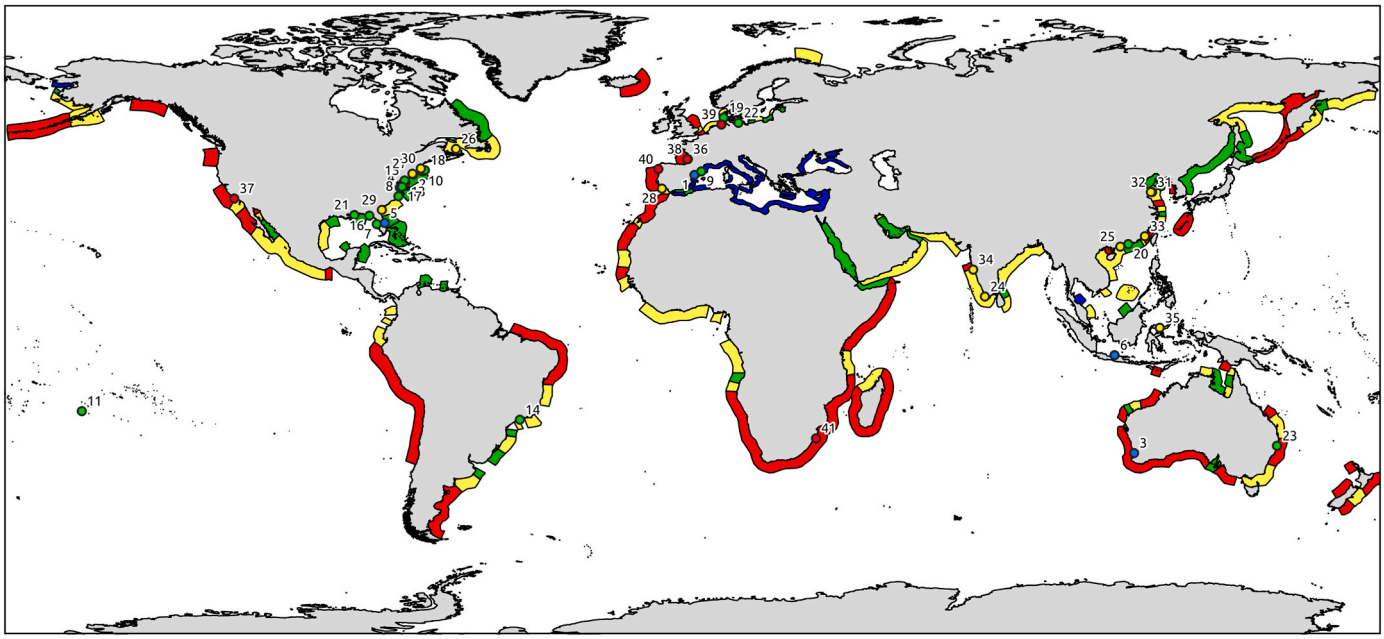

Fig. 3. Map of the distribution of sandy beach energy classes given as a function of mean tidal range and mean significant wave height as defined in Fig. 2. Blue denotes low energy, green lower moderate energy, yellow upper moderate and red high-energy conditions. Gaps indicate areas where the percentage of sandy coastline is below ~30 % in Luijendijk et al. (2018). The sites identified in our literature review where porewater studies (sampling depth >0.5 m) in sandy beach aquifers were conducted are indicated with circles, site numbers are shown according to Table 1. The local energy conditions are indicated by the color of the circle and sometimes differ from those of the map, mostly because many studies were conducted in sheltered bays. (For interpretation of the references to color in this figure legend, the reader is referred to the Web version of this article.)

yet unclear. We adopted these numbers as starting point because they have a referenced meaning for the morphological state and dynamics of barrier islands, potentially subject to revision in future studies.

Fig. 3 shows a map of the global distribution of the coastal energy classes for sandy beaches as defined above. The map is based on (i) the sandy beaches map by Luijendijk et al. (2018), (ii) mean significant wave height computed from three-hourly hindcast data (2011–2018) from the WaveWatch III® model of the US NOAA/National Weather Service for a 0.5° × 0.5° grid (WAVEWATCH III R© Development Group, 2019), (iii) mean tidal range computed from results of the DTU10 Global Tide model (Cheng and Andersen, 2011) with a grid resolution of 1.25° × 1.25°. The information was extracted at the grid elements located closest to the shoreline, and, due to the model resolution, rather represent offshore than shallow water conditions.

The map illustrates that low energy conditions (blue colors) dominate along the shorelines of marginal and inland seas such as the Mediterranean or the Black Sea. Lower moderate energy conditions (green colors) are mostly encountered at the East Coast of North America and at marginal seas like the Sea of Japan, the Red Sea, and the Persian Gulf. Most of the exposed coastlines surrounding the open oceans are either upper moderate (yellow colors) or high-energy (red colors) regimes. High-energy beaches are hence globally very common, especially in South America, Western Australia, Western Europe and Southeast Africa. Roughly, the world's sandy beaches consist of 13 % low, 23 % lower moderate, 33 % upper moderate and 31 % high-energy beaches, not taking into account sheltered bays and lagoons. In total sandy beaches make up approximately 30 % of the global coastline. Note that conditions will deviate when the resolution of the studied area is increased. For example, lower energy conditions than indicated may prevail in sheltered bays. On the other hand, higher energy conditions than indicated are possible at locations where the coastal geomorphology leads to an increase in energy. For example, tidal waves increase in convergent estuaries (Dyer, 1997) and water wave heights grow by convergent refraction in foreshore bathymetry (like the underwater canyon that creates record waves in Nazaré, Portugal (Tyler et al., 2009; Carmo, 2022). Hence, local conditions need to be accounted for when classifying a specific beach and the global map (Fig. 3) is meant to give an indication of the general distribution of the different energy regimes and not intended for inferring the energy regime of a specific site.

3. Classification of sandy beach porewater studies based on energy regime

We carried out a brief literature review on porewater studies in sandy beach aquifers, whereby we only considered studies where porewater was sampled at a depth of ≥0.5 m and the substrate was sand (i.e. STEs of sandy beaches). The threshold of 0.5 m was chosen because we consider it the minimum depth allowing for a first understanding of the coupled physical and hydrogeochemical system. Studies or sites focusing exclusively on e.g. groundwater head data, ground-based geophysics or (sediment) microbiology without any porewater sampling were not considered. We also did not take into account modelling studies without field data. As we focus on sandy beaches, studies conducted in vegetated tidal marshes (e.g. Greenwich Bay, Rhode Island, USA, Addy et al., 2005; Moses Hammock, Georgia, USA, Snyder et al., 2004; Ringkobing Fjord, Denmark, Duque et al., 2018), in estuaries (e.g. Hat Head, Australia, Sanders et al., 2017), intertidal sand banks (e.g. Moreton Bay/Island, Australia, Robinson et al., 2006) or tidal flats (e.g. Wadden Sea, Germany, Beck et al., 2008) were also not included. Similarly, studies carried out at gravel beaches (e.g. Prince William Sound, Alaska, Li and Boufadel, 2010) or in coastal aquifers but with sampling conducted only in wells inland of the beach (Motril-Salobrena aquifer, Spain, Calvache et al., 2020) were also excluded.

Based on these criteria, 41 sites (and 81 studies) in total were identified (Table 1, supplementary) which are indicated in Figs. 2 and 3. Surprisingly, local mean tidal range and wave heights are scarcely reported in many of the reviewed papers. We therefore used the DTU10 and WaveWatch III® model data to appoint each study site to its respective energy class (Table 1). For studies from sheltered bays or lagoons where no information was given on exact locations and no other data was available, a constant mean significant wave height of 0.5 m was assumed, as suggested for the Wadden Sea by (Lettmann et al., 2009). This explains the large number of studies with this particular wave height in our database. Moreover, we sometimes found a mismatch between apparent energy regimes based from regional versus local conditions. For example, several sites were at first classified as high-energy beaches based on the energy class analyses (Fig. 3), while some of them were, at closer look, in fact sheltered by islands (e.g. Cockburn Sound, Loveless and Oldham, 2010) or located adjacent to sheltered lagoons (e.g. Rarotonga, Erler et al., 2014). Consequently, the mean significant wave height was changed to 0.5 m. Therefore, the local conditions of a respective site are indicated by the circle color in Fig. 3, which sometimes differs from the regional color in the map. All sites are listed in Table 1, together with mean tidal range, mean significant wave height, resulting energy regime based on our definition (Fig. 1) and a short site description from the respective papers. In addition, the aims of each study, the porewater sampling method, maximum sampling depth and analyzed parameters are provided in an extended version of the table in the Supplementary. Note that for low-to medium-energy conditions, the search for additional studies from the respective sites was not continued, as we were aiming to identify high-energy sites. Consequently, the table was not meant to list all existing porewater studies from sandy beach aquifers and is hence not comprehensive. Sites are plotted in Fig. 2 to illustrate the energy regime of the respective beaches.

Our results show that STE porewater studies are mostly from lower to higher moderate energy conditions as defined above (Fig. 2, Table 1), while only few were conducted at high-energy conditions, even though these are globally common for sandy beaches (see red colors in Fig. 3). Specifically, 15 %, 42 % and 32 % of all identified sites were characterized by low, moderate and upper moderate energy conditions, respectively. Thus, only 12 % of all identified sites (i.e., five sites) were classified as high-energy despite our projections that more than a third of global sandy shorelines are comprised by high-energy beaches. Such an underrepresentation of study sites in contrast to global prevalence could be related to the difficulties associated with working in a high-energy environment, as well as installation, accessibility to and maintenance of scientific infrastructure.

All in all, we identified five high-energy sites, namely Santa Barbara (USA), Spiekeroog Island (Germany), Truc Vert (France), Panxón & Ladeira (Spain) and St. Lucia (South Africa) (Figs. 2 and 3). Site conditions (tidal and wave regime, morphology, geology), prevailing groundwater flow, as well as the STE biogeochemistry of these sites from the available studies are briefly summarized in the following.

4. High-energy beaches: regional and local case studies

4.1. Santa Barbara, USA

Porewater studies were conducted by Swarzenski and Izbicki (2009) and Goodridge and Melack (2014) at different beaches along the Santa Barbara channel in California, USA. The tidal range is 2 m, the mean significant wave height in the area is 1.9 m according to the WW3 model (WAVEWATCH III R© Development Group, 2019). Hence, the sites are high-energy according to our classification, though the West Beach site might be sheltered by a wharf based on an aerial picture in (Swarzenski and Izbicki, 2009). The sandy beaches in the region are rather narrow and backed by high uplifted marine terraces (Goodridge and Melack, 2014).

The urban West Beach aquifer near Santa Barbara is shallow and underlain by clay at a depth of <1 m–~10 m (Swarzenski and Izbicki, 2009). By means of inverted resistivity images Swarzenski and Izbicki

Table 1
Overview on STE porewater study sites identified in the literature, summarising information on location, mean wave height, mean tidal range, resulting energy regime based on Fig. 2 and geographical/geological site description. An extended version of the table listing all papers with respective aims, the method of porewater sampling, maximum porewater sampling depth and parameters analyzed is provided in the supplementary. Data from papers unless otherwise stated.

Site number	Site	(Connected) Sea	Longitude	Latitude	Mean wave height [m]	Mean tidal range [m]	Energy regime	Short site description	Comments	References
1	Alfacs Bay, Spain	Mediterranean Sea	0,65	40,61	0,40	0,25	low	a shallow micro-tidal semi-enclosed embayment, silty sandy sediments on top karst	wave height from WW3 model	Rodellas et al. (2017)
2	Great South Bay, New York, USA	Atlantic Ocean	−73,00	40,74	0,50	0,25	low	large shallow lagoon, bottom sediments predominantly permeable sandy glacial outwash, thickness beach aquifer 30 m	wave height from WW3 model (0.95), assumed wave height = 0.5 because sheltered bay	Beck et al. (2010)
3	Cockburn Sound, WA, Australia	Indian Ocean	115,76	−32,23	0,50	0,53	low	different sites, appear mostly sheltered, semi-enclosed marine basin/embayment, unconfined 5–10 m carbonate and silica sand underlain by 10 m limestone, thickness beach aquifer up to 30 m	assumed wave height = 0.5 because sheltered bay, tide from DTU10 Model	Taniguchi et al. (2003), Loveless and Oldham (2010), Loveless et al. (2008)
4	Gloucester point, USA	York river estuary, Atlantic Ocean	−76,51	37,25	0,30	0,80	low	sheltered bay, 20–30 m wide beach comprising fine to coarse sands, slope of approximately 0.2, bordered by marsh, granite breakwaters line beach 40 m from the dune line to prevent erosion and stabilize the beach morphology	wave height from WW3 model	O'Connor et al. (2015), Beck et al. (2016); O'Connor et al. (2018), O'Connor et al. (2022), Wilson et al. (2023)
5	Indian River Lagoon, Florida, USA	Indian River Lagoon (Atlantic Ocean)	−80,50	28,00	0,50	0,10	low	brackish lagoon with shallow water column (mean depth of 1.5 m) surrounded by pleistocene beach ridges, lagoon is underlain by a surficial aquifer mostly consisting of quartz sands	assumed wave height = 0.5 because sheltered bay	Johannesson et al. (2011), Roy et al. (2012)
6	Awur & Bandengan beach, Jepara, Indonesia	Java Sea	110,64	−6,59	0,35	0,54	low	beaches in urban bays of Jepara, coastal plain of Jepara contains alluvial products derived from redeposited volcanoclastic materials		Adyasari et al. (2019)
7	Tampa Bay, Florida, USA	Gulf of Mexico, Atlantic Ocean	−82,57	27,69	0,50	0,60	lower moderate	sheltered bay, sandy permeable soil, surficial aquifer made of sands, silts and clays, thickness of 0–28 m, 4 transects along the Pinellas shoreline	assumed wave height = 0.5 because sheltered bay, tide from DTU10 Model	Kroeger et al. (2007)
8	Neuse River Estuary, NC, USA	Atlantic Ocean	−76,91	35,00	0,50	0,60	lower moderate	two sites with sandy beaches at the eutrophic Neuse River Estuary, the second largest estuarine system in the US, unconfined, surficial aquifer that is 10–30 m thick	assumed wave height = 0.5 because sheltered bay, Tide from DTU10 Model	Null et al. (2011)

(*continued on next page*)

Table 1 (*continued*)

Site number	Site	(Connected) Sea	Longitude	Latitude	Mean wave height [m]	Mean tidal range [m]	Energy regime	Short site description	Comments	References
9	Argentona, Spain	Mediterranean Sea	2,43	41,52	0,60	0,24	lower moderate	site near the mouth of the ephemeral stream of Argentona, alluvial aquifer dominated by quaternary sediments formed by layers of gravels, sands and clays, overlyong granitic basement, 20–30 m aquifer thickness	wave height and tide range from Sayre et al. (2021); https://doi.org/10.5670/oceanog.2021.219	Martínez-Pérez et al. (2022), Ruiz-González et al. (2022)
10	Waquoit Bay, USA	Vineyard Sound, Atlantic Ocean	−70,53	41,55	0,50	1,10	lower moderate	semi-enclosed estuary, shallow unconfined aquifer, upper 10 m consists of homogeneous coarse-grained sand which is underlain by less permeable fine to very fine sand and silt	wave height from WW3 model (0.8); assumed wave height = 0.5 because sheltered bay	Talbot et al. (2003), n Mulligan et al. (2011), Charette and Sholkovitz (2006), Dulaiova et al. (2006), Gonneea et al. (2008), Kroeger and Charette (2008), Spiteri et al. (2008), Sáenz et al. (2012), Gonneea et al. (2013), Abarca et al. (2013), Liu et al. (2017)
11	Rarotonga, Cook Islands	Pacific Ocean	−159,78	−21,24	0,50	1,00	lower moderate	pacific island, STE around protected island lagoon, sediments with high porosity and hydraulic conductivity and low OM content, predominantly carbonate sands	wave height from WW3 model	Erler et al. (2014),
12	Indian River Bay, Delaware, USA	Indian River Bay, Altlantic Ocean	−75,14	38,59	0,60	1,10	lower moderate	Coastal bay	wave height from Meteorological Service of New Zealand, tide from DTU10 Model	Bratton et al. (2004)
13	Cape Henlopen, Delaware, USA	Delaware Bay, Atlantic Ocean	−75,11	38,79	0,50	1,40	lower moderate	sandy beach sheltered by Cape Henlopen, 12–18 m of very coarse sands and gravels overlie marine silts and clays, morphology of the beach consists of a dune, a 21 m wide backshore, a 14 m wide beachface with a 1:9 slope, and a broad tidal sandflat, protected from storm erosion by two offshore breakwaters	wave height from WW3 model	Ullman et al. (2003),Heiss et al. (2014), McAllister et al. (2015), Kim et al. (2017), Kim et al. (2022)
14	Flamengo Bay, Brazil	Atlantic Ocean	−45,09	−23,49	0,50	1,25	lower moderate	sandy beach overlying a fractured rock aquifer, slope ~0.044	wave height from WW3 model (0.8); assumed wave height = 0.5 because sheltered bay	Cable and Martin (2008)
15	Delmarva coastal bays, Maryland, USA	Atlantic Ocean	−75,28	39,15	0,50	1,20	lower moderate	sandy beaches adjacent coastal bays underlain by filled paleochannels	assumed wave height, tide from DTU10 Model	Bratton et al. (2004)
16	Turkey Point, Florida, USA	Gulf of Mexico, Atlantic Ocean	−84,51	29,92	0,85	0,60	lower moderate	beach with diffuse seepage near shore (from unconfined aquifer, ~2–4 m thickness) and	wave height from WW3 model	Santos et al. (2008), Li et al. (2009), Santos et al. (2009), Santos et al. (2011)

(*continued on next page*)

Table 1 (*continued*)

Site number	Site	(Connected) Sea	Longitude	Latitude	Mean wave height [m]	Mean tidal range [m]	Energy regime	Short site description	Comments	References
								submarine springs (from the confined Floridan Aquifer), silt and clay sand aquifer ontop a layered dolomite and limestone platform		
17	Chesapeake Bay, Virginia, USA	Chesapeake Bay, Atlantic Ocean	−75,96	37,48	0,50	0,70	lower moderate	tidal estuary, shallow unconfined groundwater system, partly marshland	assumed wave height = 0.5 because sheltered bay	Robinson et al. (1998)
18	Nauset Marsh, Cape Cod, USA	Atlantic Ocean	−69,96	41,83	0,50	1,34	lower moderate	several beaches of the Nauset Marsh embayment, a back-barrier estuary on Cape Cod, unconfined aquifer made of largely unconsolidated glacial sediments	assumed wave height = 0.5 because sheltered bay	Urish and McKenna (2004)
19	Ho Bay, Denmark	North Sea	8,28	55,56	0,50	1,40	lower moderate	coastal aquifer consisting of sandy sediments of Quaternary and Neogene age deposited in an up to 70 m deep buried valley cut into a thick Neogene clay deposit, secondary buried channels connect the aquifer to the coast	assumed wave height = 0.5 because sheltered bay, tide from DTU10 Model	Andersen et al. (2007)
20	Tolo Harbor, Hong Kong	South China Sea/Pacific Ocean	114,22	22,47	0,50	1,06	lower moderate	semi-closed bottlenecked embayment with six rivers discharging into it, precipitation is 2020 mm/a, shallow beach aquifer separated into several layers (sand with silt, sand with shell fragment, sand with gravel and clay)		Liu et al. (2018a); Liu et al. (2018b)
21	Gulf of Mexico beaches, USA	Gulf of Mexico, Atlantic Ocean	−88,46	30,09	0,60	0,48	lower moderate	several oil contaminated beaches on the Gulf coast (Grand Isle State Park, Bon Secour National Wild Refuge, Fort Pickens)	wave height from WW3 model, tide from DTU10 Model	Geng et al. (2021a)
22	Hütelmoor, Germany	Baltic Sea	12,16	54,22	0,64	0,15	lower moderate	rewetted coastal peatland adjacent to 40 m wide dune dike and 50 m wide beach, 0.1–1.5 m thick peat outcropping below fine to medium dune sands and marine medium to coarse sands	wave height from WW3 model, tide from DTU10 Model	Toro et al. (2022)
23	Jetty Beach, Coffs Harbour, Australia	Pacific Ocean	153,14	−30,31	0,50	1,19	lower moderate	sheltered sandy beach with a length of 0.89 km, highly affected by urban development	tide from DTU10 Model	Gómez-Alvarez et al. (2019)
24	Varkala Beach, southern India	Arabian Sea, Indian Ocean	76,70	8,73	1,20	0,60	upper moderate	major regional aquifer system (Warkali aquifer) 30 m high cliffabove a 10–100 m wide beach, in the upper 15 m of the cliff, laterites are exposed underlain by		Oehler et al. (2021)

(*continued on next page*)

Table 1 (*continued*)

Site number	Site	(Connected) Sea	Longitude	Latitude	Mean wave height [m]	Mean tidal range [m]	Energy regime	Short site description	Comments	References
								layers of sandstone and carbonaceous clay, six freshwater springs at cliff base, where the permeable sandstone overlays an impermeable clay layer		
25	Yangjiang City, Beijing Bay, China	South China Sea	112,13	21,80	0,71	1,56	upper moderate	due to the construction of embankment, only limited exchange between bay water and open sea water, sandy beach acting as shallow unconfined aquifers, less permeable layer is between ~7 and ~9 m	wave height from WW3 model	Wang et al. (2023), Zhang et al. (2024)
26	Martinique Beach (Îles-de-la-Madeleine, Canada)	Gulf of St-Lawrence, Atlantic	−61,82	47,40	1,10	0,56	upper moderate	sandy barrier systems with fine-grained sands ontop sandstone aquifer, sandy beach acts as shallow unconfined aquifer	wave height from WW3 model, tide from DTU10 Model	Chaillou et al. (2016); Couturier et al. (2016); Couturier et al. (2017); Chaillou et al. (2018); Sirois et al. (2018)
27	Smithtown Bay, Long Island, USA	Long Island Sound, Atlantic Ocean	−73,23	40,91	0,30	2,10	upper moderate	Callahan's Beach: coastal bluff with a large terrestrial hydraulic gradient, coarse-grained sand; Long Beach: barrier beach, coarse-grained sand to pebbles and cobbles		Tamborski et al. (2017)
28	Ria Formosa, Portugal	Ria Formosa, Atlantic Ocean	−7,89	37,01	0,50	2,14	upper moderate	inner intertidal area of the Ancao peninsula at the mesotidal Ria Formosa coastal lagoon, medium-coarse sand, beach slope 10.4 %	wave height from WW3 model (1.3); assumed wave height = 0.5 because sheltered bay, Tide from DTU10 Model	Ibánhez and Rocha (2016)
29	Cabretta Island, Georgia, USA	Atlantic Ocean	−81,24	31,43	0,75	2,50	upper moderate	beach on small Holocene transgressive barrier island, fine sands with irregularly distributed mud and silt layers, confining unit at appr. 3 mbgs with confined aquifer below	wave height from WW3 model	Evans and Wilson (2017)
30	Quincy Bay, Massachusetts, USA	Massachusetts Bay, Atlantic Ocean	−71,02	42,28	0,50	2,90	upper moderate	tidal bay bordered by tidal flats and beaches, 1,5 m siliciclastic muddy fine sand on top of bedrock	assumed wave height (WW3 model offhore = 0.83) = 0.5 because sheltered bay	Poppe and Moffett (1993)
31	Shilaoren Beach, Qingdao, China	Yellow Sea	120,47	36,09	0,50	2,50	upper moderate	beach with 30–40 m intertidal zone, layered beach sediments made of 3–5 m of medium-coarse sand over 1.5–2.0 m of pebble, on top medium-fine sand, then 0.2–1.3 m of silty fine sand, then gravel sand	wave height from WW3 model, tide from DTU10 Model	Zhang et al. (2021)
32	Jiaozhou Bay, China	Yellow Sea	120,15	36,09	0,50	2,71	upper moderate	semi-enclosed bay, located at the southeast of	assumed wave height = 0.5	Qu et al. (2017)

(*continued on next page*)

Table 1 (*continued*)

Site number	Site	(Connected) Sea	Longitude	Latitude	Mean wave height [m]	Mean tidal range [m]	Energy regime	Short site description	Comments	References
								Shandong Peninsula, extensive surf zone where waves dissipate most of their energy before reaching the shoreline	because sheltered bay	
33	Weitou Bay, Fujian, China	South China Sea	118,58	24,52	0,96	2,50	upper moderate	coarse-grained, highly permeable sands	wave height from WW3 model	Cai et al. (2020)
34	North Goa and Sindhudurg beaches, India	Arabian Sea, Indian Ocean	73,64	15,77	1,32	1,45	upper moderate	several beaches along 171 km at the west indian coast, average of 2840.0 mm/a of rainfall within four months, low topography, area covered by fractured basalt in Sindhudurg and Precambrian rocks with intruded dykes in North Goa, mostly lateralized and covered with soil and alluvium	wave height from WW3 model, tide from DTU10 Model	Prakash et al. (2024)
35	Shengsi Island, China	East China Sea	122,47	0,55	0,55	2,22	upper moderate	no site infos	wave height from WW3 model, tide from DTU10 Model	Chen et al. (2020)
36	Cassy Beach, France	Arcachon Beach, Atlantic Ocean	−1,10	44,71	0,50	2,90	upper moderate	mesotidal, shallow lagoon, lower part of the intertidal zone consists of muddy sediments, upper parts are made of permeable, sandy sediments	tide from DTU10 Model, assumed wave height = 0.5 because sheltered bay	Delgard et al. (2012)
37	Santa Barbara, USA	Pacific Ocean	−119,89	34,41	1,90	2,00	high	shallow (0.4–2.3 m) unconsolidated medium sized sand ontop of bedrock, 10–55 m beach width till marine cliffs	wave height from WW3 model, According to an offshore boye STATION 46053 in St. Barbara Channel monthly 1.0–1.6	Goodridge and Melack (2014), Swarzenski and Izbicki (2009),
38	Truc Vert, France	Altlantic Ocean	−1,25	44,72	1,50	3,20	high	French Aquitanian coast is 250-km long straight coast bordered by high aeolian dunes, double bar beaches with very dynamic rhytmic features; unconsolidated medium sized sand		Anschutz et al. (2009), Charbonnier et al. (2013), Buquet et al. (2016); Charbonnier et al. (2016), Anschutz et al. (2016), Charbonnier et al. (2022)
39	Spiekeroog, Germany	North Sea, Altlantic Ocean	7,71	53,78	1,20	2,70	high	barrier island sandy beach bordered by aeolean dunes, foreshore dissected by a ridge and runnel system, 40–50 m beach aquifer thickness	wave height from WW3 model	Reckhardt et al. (2015), Ehlert et al. (2016), Beck et al. (2017), Reckhardt et al. (2017), Waska et al. (2019a), Degenhardt et al. (2020, 2021a,b), Grünenbaum et al. (2020a), Grünenbaum et al. (2020b), Paffrath et al. (2020), Ahrens et al. (2020, 2021)
40	Panxon & Ladeira, Spain	Ría de Vigo, Atlantic Ocean	−8,83	42,13	1,90	2,30	high	two sandy beaches in Baiona Bay, Panxton is more exposed, surrounded by metasedimentary	wave height from WW3 model, tide from DTU10 Model	Calvo-Martin et al. (2021); Calvo-Martin et al. (2022)

(*continued on next page*)

Table 1 (*continued*)

Site number	Site	(Connected) Sea	Longitude	Latitude	Mean wave height [m]	Mean tidal range [m]	Energy regime	Short site description	Comments	References
								formation dominated by shales with intrusions of igneous rocks such as granite, pegmatite, pegmaplite and quartz		
41	St. Lucia Estuary, South Africa	Indian Ocean	32,43	−28,37	1,92	1,42	high	several beaches along a stretch of land between Lake St. Lucia, Lake Sibaya and Kosi Bay, sandy beaches underlain by fractured bedrock	wave height from WW3 model, tide from DTU10 Model	Moore et al. (2019)

(2009) describe a freshwater body at 15 m depth below the high-water line moving significantly between high- and low tide, but no classical USP. The role of the clay in the groundwater distribution patterns remains unclear. The beach aquifers (Gaviota, Isla Vista, Manzanita, East Campus) studied by Goodridge and Melack (2014) are shallow and comprised of an unconsolidated medium sized sand layer with only 0.4–2.3 m thickness on top of bedrock. Using ^{222}Rn, porewater residence times of 4.4–6.4 days for the shallow beach porewaters were calculated.

Beach porewaters contained mainly ammonia as dissolved inorganic nitrogen (DIN), more dissolved organic carbon (DOC) and less dissolved oxygen than seawater (Goodridge and Melack, 2014). SGD was postulated a sustained source for nutrients to the coastal sea (Swarzenski and Izbicki, 2009) and the temporal variability in DIN fluxes to the ocean was found to be significant (Goodridge and Melack, 2014). In both studies, there was very little freshwater influence in the SGD. The studies focused on temporal variability of very shallow, young porewaters, and fluxes from shallow and narrow beaches. Further studies from the Santa Barbara beaches focused on the role of macrophyte wrack inputs and dissolved nutrients on porewater in open shallow dug pits (Dugan et al., 2011) and the influence of SGD on nearshore DOC reactivity, concentration dynamics, and offshore export (Goodridge, 2018). Nevertheless, distribution patterns of porewater constituents associated with STE hydrology remain largely unknown.

4.2. *Truc Vert, France*

Truc Vert is the main beach that was extensively studied along the French Aquitanian coast, a 250 km stretch of straight high-energy Atlantic coast beaches between the Gironde and Adour estuaries with little direct anthropogenic influence (Charbonnier et al., 2022). The Truc Vert beach is 80–200 m wide in cross-shore direction and aligned by aeolian dunes several tens of meters high (Anschutz et al., 2016). The beach, consisting of medium sized sand, is located north of the Cap Ferret Spit. The upper 40 m of the beach aquifer consist of marine, lake and river deposits and the transmissivity is high, while at −30 to −40 m, a less permeable more clayey layer from the Pliocene is present (Buquet et al., 2016 and references therein). Morphologically, Truc Vert beach consists of a dynamic double bar system and ridge and runnel systems. The tidal range is 3.2 m and up to 5 m during spring tides, mean significant wave height is 1.5 m but waves can reach up to 10 m during winter storm surges (Anschutz et al., 2009; Buquet et al., 2016; Charbonnier et al., 2013). Accordingly, it is clearly high-energy. Charbonnier et al. (2013) report on topography variations over almost 2 years along a cross-shore transect, with ground elevation sometimes varying >1 m between two successive campaigns only 2 weeks apart, caused by longshore migration of the ridge and runnel system.

In porewaters retrieved from boreholes of up to 1.2 m depth, Anschutz et al. (2009) found a successive enrichment of silica concentrations along a cross-shore transect from the upper towards the lower beach prior to discharge. Estimated residence times are as low as 3.5 days, similar for three sampling events. Buquet et al. (2016) conducted electrical resistivity tomography (ERT) from the dune base to just above the MWL supported by measured salinities and identified an almost vertical stable freshwater-saltwater transition zone at the upper beach, controlled by spring tide levels.

Anschutz et al. (2009) state that porewater has salinities similar to seawater but is reduced in dissolved oxygen and contains higher concentrations of nitrate and inorganic phosphorous besides silica. They conclude that the sands act as biogeochemical reactors. Charbonnier et al. (2013) investigated the seasonality of aerobic respiration and found that the most intense oxygen depletion occurs in spring, when planktonic OM is most abundant as well as in summer, when denitrification also occurs. Mass fluxes calculated for the entire coast (Charbonnier et al., 2013) revealed that cross-shore variations are far more pronounced than longshore variations. Charbonnier et al. (2013) also highlight the fact that topography variations affect porewater chemistry at the meter scale and that there is continuous sediment movement. The study by Anschutz et al. (2016) focusses on freshwater SGD and associated nutrient discharge along the entire Aquitanian coast between the beaches of Le Gurp and Tarnos. Brackish water was detected at all beaches, mainly at the lower beach, the seeps and the runnel, indicating mixing of circulating seawater with fresh terrestrial groundwater within the STE. Freshwater endmembers are enriched in nitrate, phosphate, ammonium and dissolved silica and a redox boundary suspected below the foredune inland of the salinity boundary. Anschutz et al. (2016) conclude that fresh SGD is a nutrient source, however only a minor one in comparison to river inputs, as the terrestrial SGD is only a minor fraction in the water budget and the local forested land use is not a major nutrient supplier. Charbonnier et al. (2022) studied carbon dynamics at Truc Vert and budgeted carbon fluxes via SGD for the entire Aquitaine coast. DOC is decreasing while DIC is increasing from upper to lower beach which is related to aerobic respiration of trapped marine OM within the beach (Charbonnier et al., 2022). They also noted strong temporal variability in DIC, dissolved oxygen, DOC and computed CO_2 pressures on tidal and seasonal time scales and major hydrochemical changes from the terrestrial groundwater to the beach (oxidation of reduced iron and ammonium, degassing of CO_2). A major conclusion is that high-energy beaches deliver DIC into the coastal ocean together with a surplus of total alkalinity, which increases the buffering capacity against ocean acidification. Likewise, they deliver CO_2 to the atmosphere and should hence be accounted for in carbon budgets.

4.3. Spiekeroog, Germany

Spiekeroog is a barrier island in the southern North Sea in front of the North-German coastline. In the north, the island is exposed to waves with mean significant wave heights of 1.4 m coming mostly from the North-West (Herrling and Winter, 2017, 2018). The semidiurnal tides have a tidal range of 2.7 m (Beck et al., 2017), hence Spiekeroog's northern beach is high-energy based on our classification. Regular storm floods add to the dynamics, with offshore waves reaching up to 11 m during storm conditions (Dobrynin et al., 2010). Typical beach features are a constantly reshaping ridge and runnel system parallel to the shoreline (Dobrynin et al., 2010), confirmed by repetitive LIDAR scanning of the intertidal zone by Grünenbaum et al. (2020a). The northern beach is comprised of mostly fine to medium sized quartz sands with finely dispersed or interlayered shells or shell debris (Beck et al., 2017). The beach aquifer reaches down to 44–55 m below ground surface (mbgs), where it is underlain by a rather continuous clay layer (Röper et al., 2012).

Knowledge on groundwater flow and transport patterns is based on numerical modelling by (Beck et al., 2017; Grünenbaum et al., 2020b), in combination with shallow groundwater salinity and age data from temporally installed wells (Grünenbaum et al., 2020b) as well as high-density shallow (1 m deep) porewater sampling in the intertidal zone with porewater lances (Waska et al., 2019b). SGD with a freshwater component discharges both in intertidal runnels and near the LWL, accompanied by at least two saltwater circulation cells at the time (Waska et al., 2019b; Grünenbaum et al., 2020a). Multiple, 10–20 m deep saltwater circulation cells aligning discharge zones were visible in cross-shore ERT (Grünenbaum et al., 2023) and the discharging water at the LWL is up to 21 years old (Grünenbaum et al., 2020b). Beach topography clearly affects groundwater flow and transport in the STE, as net exfiltration only occurs at the topographic lows that are constantly reshaped (Grünenbaum et al., 2020a).

The porewater biogeochemistry of Spiekeroog shows a distinct cross-sectional redox zonation, whereby oxic conditions prevail in the supratidal and around the MHWL up to 2 m depth (Reckhardt et al., 2015; Beck et al., 2017). Dissolved oxygen concentrations rapidly decrease towards the lower intertidal zone and are overall low to zero below the MWL, where sediments are mostly water-saturated (Beck et al., 2017; Ahrens et al., 2020). High nitrate concentrations are present in the supra- and upper intertidal and manganese, iron and ammonium concentrations increase downstream along the flowpaths in the USP. Sulfide was only detected at trace amounts around the LWL. Although pyrite occurs in sediments of the same beach stretch further east (Seibert et al., 2019) and sulfate-reducing microbes were reported from the site (Beck et al., 2017; Degenhardt et al., 2020), sulfate reduction rates seem to be extremely low (Beck et al., 2017; Ahrens et al., 2020).

Microbial community compositions studied within the shallow subsurface (0–1 mbgs) are overall structured according to the prevailing redox regimes (Degenhardt et al., 2020). DOM in intertidal porewaters is mainly of marine origin, with additional terrestrial contributions from the local freshwater lens at the upper beach and at the LWL (Beck et al., 2017; Waska et al., 2021). Porewater DOM compositions (Waska et al., 2019b) are associated to metabolically different bacterial clusters which show distinct cross-shore and depth zonations (Degenhardt et al., 2021b). Within shallow sediments (0.3–1 mbgs) of the upper beach, members of the candidate phyla radiation (CPR), ultra-small Gammaproteobacteria, and several autotrophic bacteria are related to recalcitrant DOM compounds. SGD-impacted deeper sediments of the lower beach showed a correlation of small, partially terrestrial-derived DOM compounds and *Dehalococcoides* species. Furthermore, DOC distributions, together with high oxygen consumption rates derived from in situ data and incubations, revealed a fast and efficient OM turnover in this system (Reckhardt et al., 2015; Beck et al., 2017; Ahrens et al., 2020; Waska et al., 2021). Fresh OM like algal polymers (e.g. alginate and carrageen) are presumably degraded within the uppermost sediments across the intertidal zone by *Flavobacteria* species (Degenhardt et al., 2021b). Overall, the beach STE appears to be a net sink for DOM and redox-sensitive metals like rhenium, uranium and vanadium, and a net source for nutrients, iron, manganese, and rare earth elements (Reckhardt et al., 2017; Beck et al., 2017; Ahrens et al., 2020; Paffrath et al., 2020).

4.4. Panxón and Ladeira, Spain

Two different beach sites, Panxón and Ladeira, were recently reported on in the Ría de Vigo, a large coastal inlet at the NW Iberian Peninsula by (Calvo-Martin et al., 2021, 2022). According to the WW3 and DTU10 models (Table 1), the sites are clearly high-energy. Baiona Bay, where the beaches are located, is wave-dominated and exposed to energetic waves when the wind direction is westerly and southwesterly in winter. Semindurnal tides have a range of 3–3.5 m during spring and 1.5–2 m during neap tides respectively (Calvo-Martin et al., 2021 and references therein). The reflective Ladeira beach is more protected than the dissipative Panxón beach. Both beaches consist of siliciclastic sands with carbonates and are homogenous with the exception of a shallow gravel layer at Panxón beach. The beaches are surrounded by hardrock (metasedimentary formation dominated by shales with intrusions of igneous rocks) and have been altered by humans (Calvo-Martin et al., 2021 and references therein), whereby the beach thickness is unclear. Beach profiles that were measured four times over a year show distinct topography variations.

Shallow (up to 1.8 mbgs) porewater salinities are low compared to seawater, confirming freshwater inflow to the beaches. Site specific seasonal salinity variations are likely due to differences in circulation patterns and freshwater supply (Calvo-Martin et al., 2021). At both sites, a shallow (~1 m) USP and a saltwater wedge separated by a freshwater tube were identified, yet the USP is somewhat distorted by the gravel layer at Panxón which is causing preferential flow. Size and position of the USP vary as a function of meteoric freshwater inflow and wave forcing, whereby the comparatively deeper USP at Panxón was attributed to the more intense wave forcing (Calvo-Martin et al., 2021). Transit times estimated with ^{222}Ra are in the order of days to weeks.

Nutrient biogeochemistry and microbial ecology of the STEs was studied by Calvo-Martin et al. (2021, 2022) respectively. Redox conditions are mostly oxic at Panxón and suboxic to anoxic at Ladeira. The gradients of oxygen, nitrate and ammonium are largely related to groundwater flow within the STE, whereby the USP continuously pumps oxygen and OM into the beach aquifers, causing aerobic respiration of OM as well as nitrification of the produced ammonium. Nutrients are partly provided by meteoric freshwater. POM is trapped in the shallow sediment during infiltration, leading to oxygen consumption, denitrification of freshwater-derived nitrate and ammonium accumulation in the shallow STE (Calvo-Martin et al., 2021).

The microbial community in the STE is highly diverse, even and rich and characterized by a mixture of cosmopolitans and rare taxa, whereby it differed mostly between shallow and deep sediment layers (Calvo-Martin et al., 2022). The microbial community structure is linked to the biogeochemistry, yet in contrast to the transient geochemistry remarkably stable over the seasons and along beach profiles (Calvo-Martin et al., 2022). The more oxic Panxón beach aquifer shows strong associations between heterotrophs and autotrophic nitrifiers, overall archaea, and acts as a net source of nitrogen to the coast (Calvo-Martin et al., 2021, 2022). In contrast, the more anoxic Ladeira beach aquifer is effectively a net nitrogen sink (Calvo-Martin et al., 2021) and the microbial community dominated by anaerobic heterotrophs (e.g. Dehalococcoidia and Desulfatiglans), giving evidence to the degradation of complex and aromatic compounds as well as the co-occurrence of methane oxidizers and methanogens (Calvo-Martin et al., 2022).

4.5. St. Lucia, South Africa

The only study from the area by Moore et al. (2018) is also the only beach porewater study we found from the African continent, despite a prominence of high-energy shorelines according to our new classification scheme (Fig. 3). Various beaches along a long coastal stretch between the St. Lucia Estuary and Kosi Bay were sampled using push-point devices up to a depth of ~2 m, at which depth often the bedrock was encountered. The beach locations are mostly between lakes (Lake St. Lucia, Lake Sibaya and Kosi Bay) and the sea, separated by a 100- to 140-m-high vegetated dune barrier. According to the WW3 and DTU10 models, regional mean wave height and tidal range at the beach locations are 1.92 m and 1.42 m respectively, which indicates high-energy conditions. In the area, an extensive unconsolidated aquifer is underlain by consolidated Cretaceous siltstones and the coastal lakes are located in palaeovalleys that were excavated into the bedrock during the last glacial maximum (Moore et al., 2018).

Moore et al. (2018) used radium isotopes to study SGD and related mixing within the respective beaches to estimate SGD water and nutrient fluxes to the coastal sea. Porewater residence times range from 0.3 to 2.3 days and this rapid flushing delivers nutrients to the sea. Extremely high activities of ^{224}Ra relative to ^{228}Ra were measured, far above those elsewhere in the world, which the authors attribute to different groundwater components flowing into the system. Moore et al. (2018) suspect that significant amounts of nutrients are supplied to the ocean via flow underneath the beaches in deeper paleochannels, at depths not reached by the beach sampling. They therefore call for more research and permanent infrastructure in the area.

5. Site comparison and methodological challenges encountered at high-energy sites

Despite some differences in wave conditions and beach shape, the sites Truc Vert and Spiekeroog are comparable regarding sedimentology, hydro- and morphodynamics, and represent thick beach aquifers bordered by extensive dunes. In contrast, the beach aquifers at the St. Barbara and St. Lucia sites are very shallow and on top of consolidated bedrock. The thickness of the Panxón and Ladeira beach aquifers is not given, yet the sites are also surrounded by hardrock. Hence fundamental differences in the geology underlying the sandy beaches exist, which likely impacts on groundwater flow and transport.

At Spiekeroog and Truc Vert, authors stated that beach morphology controls discharge (Anschutz et al., 2016; Grünenbaum et al., 2020a; Waska et al., 2019b) and also varies strongly over short time intervals (Charbonnier et al., 2013; Greskowiak and Massmann, 2021). For example, Castelle et al. (2007) reported that the beach surface elevation at Truc Vert can vary up to 3 m following storms within a few weeks. The strong beach morphodynamics observed at Truc Vert and Spiekeroog reflect the findings of Blossier et al. (2016, 2017), who reported that tidal and wave forcing shape high-energy beaches on short time scales. Furthermore, both sites have in common that also the width of the intertidal zone varies considerably as a function of topography, tidal range and wave regime (Charbonnier et al., 2022). Similarly, beach profile measured repeatedly by Calvo-Martin et al. (2021) showed variations in topography of $>$ 1m between campaigns and Swarzenski and Izbicki (2009) also note that the beach front and seepage face move seasonally due to sand accumulation on the beach. Regarding the proposed morphology-dependent transient flow and transport with deep and dynamic saltwater circulation in the beach aquifer (Fig. 1), there is indication from geophysical imaging at Spiekeroog that the USP is deep and indeed consists of multiple cells discharging towards the topographic lows (Grünenbaum et al., 2023). As Anschutz et al. (2016) detected brackish water mainly at the lower beach, the seeps and the runnel of beaches along the coastline, it can be speculated that this might also support the conceptual idea of a more transient high-energy STE presented in Fig. 1. However, the spatially-temporally resolved data to confirm such a concept is presently missing for all high-energy sites, as is data from greater depths.

Considerable amounts of sediment can be mobilised and deposited at high-energy beaches, sometimes within only a few hours (i.e. during tidal inundation or a storm event). As such, methodological challenges encountered at high-energy sites are a direct consequence of these harsh conditions which frequently cause the destruction of equipment. The fact that sediment is permanently relocated also requires high frequency of morphological mapping and makes the positioning of fixed installations a challenge, as they observe different morphological zones, depending on their relative position to the beach system. For example, Charbonnier et al. (2013) reported that any attempts to build piezometric wells at Truc Vert failed because they were quickly broken, buried or filled with sand, according to Charbonnier et al. (2022) sometimes even after only one tidal cycle. Therefore, authors relied on water collected from open holes dug to the top of the water table during low tide. Anschutz et al. (2016) installed 7 m deep supratidal wells between the spring tide line and the dunes, but ruled out the installation of piezometers in the intertidal zone, as did Buquet et al. (2016) and Charbonnier et al. (2022) because of the rough high-energy conditions at Truc Vert. Though problems with infrastructure are not specifically discussed, installations of piezometers and push-points samplers at beaches at Spiekeroog (Grünenbaum et al., 2020a), Panxón and Ladeira (Calvo-Martin et al., 2021) and St. Lucia (Moore et al., 2019) were only done for the duration of a campaign. Swarzenski and Izbicki (2009) installed permanent piezometers above the high water line and a temporal well near the intertidal zone without reporting on any infrastructural problems. Only very recently, Massmann et al. (2023) installed four wells of up to 24 m depth in the intertidal zone of Spiekeroog, which was, however, very costly and challenging, as the non-inundated time was simply too short for conventional land-based drilling in the intertidal zone. Drilling for the well at the low water line hence had to be done from a drilling barge that could operate throughout a tidal cycle. The ship used two pole anchors to stabilize, allowing it to move up and down with the tides without losing position. The installation was delayed several times as the ship could only reach the beach during calm seas when wave heights were below 0.5 m, which is rarely the case at this site. The intertidal wells on Spiekeroog are fully submersed twice a day and are still operational after ~2 years, but opening the lids is often difficult as they get blocked by barnacles and sediment and any metal bits like screws corrode quickly by saltwater. Also, the surface elevation in the intertidal zone changes often due to sediment transport, hence wells occasionally have to be extended or shortened. Equipment at a nearby pole that is also located in the intertidal zone on Spiekeroog to measure wave heights and monitor the beach with cameras (Massmann et al., 2023), faces harsh conditions and a mounted wind generator broke three times in 1 ½ years in severe gusts.

According to Anschutz et al. (2016), flux estimates are also challenging under high-energy conditions subject to tidal currents and breaking waves and more difficult than at water bodies with limited circulation. Authors concluded that both the use of Ra/Rn tracers and the application of seepage meters are more suitable for calm conditions and strongly limited at high-energy beaches. Grünenbaum et al. (2020a) applied seepage meters on Spiekeroog beach, however only at times when conditions were rather calm. A seepage meter that was installed at the site to measure SGD fluxes over several weeks was buried under sand from a moving ridge. It could not be recovered using by manually shoveling because ~0.8 m of saturated sand were sitting on top three weeks after installation close to the LWL. An attempt to apply a metal ring (~1.5 m diameter) and pumps to recover the sand on top of the seepage meter failed, because the sand-water mixture continuously flowed upwards within the ring, making it impossible to recover the seepage meter. Over a period of about one year, the height of the sand column above of the seepage meter varied between 0.6 and 1.1 m. The seepage meter finally reappeared in 2023 following erosion after having been buried for almost 3 years in the sand. A lander system was also

deployed at the runnel at a campaign on Spiekeroog beach. The lander was fixed with 80 kg of concrete weights, since the control unit was installed in a tube that was partially filled with air. Despite the additional weight, the lander moved approx. 100–150 m in a southeasterly direction along shore within one tidal cycle.

Another complication at some beaches is artificial sand nourishment for coastal defense. Sand can be supplied below the low water line (leaving it to the currents to distribute the sand along the coast), on the beach itself or the foredunes. While not unique to high-energy beaches, sand nourishment tends to be more frequent and intense here as erosion rates are high. It forms a significant factor in shaping the beach morphology but also affects the sediment geochemistry (Pit et al., 2017), potentially adding another layer of complexity to the study of high-energy STEs.

According to Calvo-Martin et al. (2022), an accurate characterization of the spatiotemporal variability of the microbial community structure in STEs is hindered by the sediment heterogeneity and more STE specific, the large, oscillating biogeochemical gradients in this environment.

As very few high-energy sites have been studied so far, the functioning of high-energy beaches still remains largely unknown, in particular where difficult to reach, i.e. at greater depths and towards the LWL. So far, most high-energy studies were focused on calculating mass fluxes of water and solutes to coastal waters (Anschutz et al., 2009; Swarzenski and Izbicki, 2009; Charbonnier et al., 2013; Goodridge and Melack, 2014; Buquet et al., 2016; Beck et al., 2017; Moore et al., 2018; Grünenbaum et al., 2020a), rather than on processes within the STE itself. It is therefore at this stage not possible to infer on spatially resolved reactive transport processes within high-energy beaches, as the spatially and temporally resolved data needed for this is mostly lacking. Furthermore, none of the high-energy studies carried out dedicated numerical modelling to resolve transient reactive transport patterns in the field, yet such coupling of biogeochemical processes with the underlying physical processes is urgently needed and the key to ultimately unravel the role of the STE in controlling geochemical fluxes to the sea.

6. Conclusions and limitations

In this paper, we present a new, simple classification scheme for the energy state of beaches that accounts for the combined effect of significant mean wave height and mean tidal range and provide a global map on coastal energy regimes. We review and classify existing porewater studies from sandy beach aquifers based on their energy regime. We hypothesize that the energy state is relevant for the biogeochemical functioning of beach aquifers, yet boundary conditions are often not reported on. We encourage authors to account for these conditions, i.e. mean significant wave heights and mean tidal range, in future studies.

So far, most research involving porewater analysis of beach aquifers has focussed on moderate energy sites. High-energy sites, in particular at greater sediment depths, have hardly been investigated. Therefore, the understanding of the functioning of high-energy beaches is limited to and based on very few sites. As the research methods applied at these sites differed and covered mostly shallow aquifer depths, it is, at this stage, not possible to derive general conclusions on the functioning of high-energy systems from the few existing studies. Yet, the fact that the morphology varies strongly and dynamically at high-energy beaches is in fundamental contrast to the situation at lower energy sites, where morphological changes are far less pronounced. The proposed transient nature of groundwater flow and transport caused by morphodynamics and stormfloods based on numerical models cannot be fully confirmed by in situ data at this stage, although complex salinity distribution patterns were found in some field studies and high seawater volume flow caused by tidal and wave pumping is likely. The biogeochemical functioning and associated chemical fluxes of high-energy beach aquifers are presumably highly complex and demand further research efforts. Because of the high seawater volume flow, a high potential for OM input and carbon remineralization can be expected.

Methodological challenges encountered when studying high-energy beach aquifers are large and involve the frequent destruction of research equipment, while the installation of permanent infrastructure is costly and difficult. Despite these challenges, beach research at high-energy sites is nevertheless timely, as high-energy beaches are representative of a large part of global shorelines and may bring up hitherto unexplored characteristics.

It was beyond the scope of this study to compare beach aquifers from different energy states based on all porewater studies listed. Hence, future research efforts should aim at highlighting the similarities and/or differences across different energy regimes as well as elucidating their respective global relevance. A clear limitation of the proposed classification is that it only considers two parameters, namely mean tidal range and mean significant wave height. It neglects other obvious factors that affect the flow and transport patterns in the STE, e.g., hydraulic conductivity, porosity, aquifer depth, beach slope, meteoric groundwater discharge, or spring-neap tide characteristics. Data of these parameters on the global scale, however, is very limited and subject to tremendous uncertainty, even though a lot of progress was made in the recent years to generate these datasets (e.g., Zarmsky et al., 2018; Luijendijk et al., 2020; Moosdorf et al., 2024). If and how these other parameters can be incorporated into a STE classification scheme requires more in-depth investigations and is beyond the scope of the present study. Hence, the classification is only a first attempt to systematically account for the environmental conditions in beach aquifer porewater studies. Other important factors such as the geological conditions should be added in future studies to develop the proposed classification further for a more holistic categorisation.

CRediT authorship contribution statement

Gudrun Massmann: Writing – original draft, Methodology, Funding acquisition, Data curation, Project administration, Investigation, Formal analysis, Conceptualization. **Janek Greskowiak:** Writing – original draft, Data curation, Methodology, Funding acquisition, Investigation, Formal analysis, Conceptualization, Visualization. **Julius Degenhardt:** Writing – review & editing, Conceptualization. **Bert Engelen:** Funding acquisition, Writing – review & editing, Conceptualization. **Moritz Holtappels:** Funding acquisition, Writing – review & editing, Conceptualization. **Rena Meyer:** Writing – review & editing, Conceptualization. **Mike Müller-Petke:** Writing – review & editing, Funding acquisition, Conceptualization. **Nils Moosdorf:** Writing – review & editing, Conceptualization. **Jutta Niggemann:** Funding acquisition, Writing – review & editing, Conceptualization. **Katharina Pahnke:** Funding acquisition, Writing – review & editing, Conceptualization. **Vincent Post:** Funding acquisition, Writing – review & editing, Conceptualization. **Anja Reckhardt:** Funding acquisition, Writing – original draft, Conceptualization. **Kai Schwalfenberg:** Writing – review & editing, Conceptualization. **Stephan Seibert:** Writing – review & editing, Conceptualization. **Hannelore Waska:** Writing – original draft, Funding acquisition, Conceptualization. **Christian Winter:** Writing – review & editing, Funding acquisition, Conceptualization.

Funding

This study was conducted within the research unit FOR 5094: The Dynamic Deep subsurface of high-energy beaches (DynaDeep), funded by the German Research Foundation (Deutsche Forschungsgemeinschaft, DFG). We thank all DynaDeep colleagues and cooperator for fruitful discussions.

Declaration of competing interest

The authors declare that they have no known competing financial interests or personal relationships that could have appeared to influence

the work reported in this paper.

Appendix A. Supplementary data

Supplementary data to this article can be found online at https://doi.org/10.1016/j.ecss.2025.109424.

Data availability

No data was used for the research described in the article.

References

Abarca, E., Karam, H., Hemond, H.F., Harvey, C.F., 2013. Transient groundwater dynamics in a coastal aquifer: the effects of tides, the lunar cycle, and the beach profile. Water Resour. Res. 49 (5), 2473–2488.

Addy, K., Gold, A., Nowicki, B., McKenna, J., Stolt, M., Groffman, P., 2005. Denitrification capacity in a subterranean estuary below a Rhode Island fringing salt marsh. Estuaries 28 (6), 896–908.

Adyasari, D., Oehler, T., Afiati, N., Moosdorf, N., 2019. Environmental impact of nutrient fluxes associated with submarine groundwater discharge at an urbanized tropical coast. Estuar. Coast Shelf Sci. 221, 30–38.

Ahrens, J., Beck, M., Böning, P., Degenhardt, J., Pahnke, K., Schnetger, B., Brumsack, H. J., 2021. Thallium cycling in pore waters of intertidal beach sediments. Geochem. Cosmochim. Acta 306, 321–339.

Ahrens, J., Beck, M., Marchant, Hannah K., Ahmerkamp, S., Schnetger, B., Brumsack, H.-J., 2020. Seasonality of organic matter degradation regulates nutrient and metal net fluxes in a high energy sandy beach. J. Geophys. Res.: Biogeosciences 125 (2), e2019JG005399.

Andersen, M.S., Baron, L., Gudbjerg, J., Gregersen, J., Chapellier, D., Jakobsen, R., Postma, D., 2007. Discharge of nitrate-containing groundwater into a coastal marine environment. J. Hydrol. 336 (1), 98–114.

Anschutz, P., Charbonnier, C., Deborde, J., Deirmendjian, L., Poirier, D., Mouret, A., Buquet, D., Lecroart, P., 2016. Terrestrial groundwater and nutrient discharge along the 240-km-long Aquitanian coast. Mar. Chem. 185, 38–47.

Anschutz, P., Smith, T., Mouret, A., Deborde, J., Bujan, S., Poirier, D., Lecroart, P., 2009. Tidal sands as biogeochemical reactors. Estuar. Coast Shelf Sci. 84 (1), 84–90.

Anwar, N., Robinson, C., Barry, D.A., 2014. Influence of tides and waves on the fate of nutrients in a nearshore aquifer: numerical simulations. Adv. Water Resour. 73, 203–213.

Archana, A., Francis, C.A., Boehm, A.B., 2021. The beach aquifer microbiome: research gaps and data needs. Front. Environ. Sci. 9, 13.

Beck, A.J., Cochran, J.K., Sanudo-Wilhelmy, S.A., 2010. The distribution and speciation of dissolved trace metals in a shallow subterranean estuary. Mar. Chem. 121 (1–4), 145–156.

Beck, A.J., Kellum, A.A., Luek, J.L., Cochran, M.A., 2016. Chemical flux associated with spatially and temporally variable submarine groundwater discharge, and chemical modification in the subterranean Estuary at Gloucester point, VA (USA). Estuaries Coasts 39 (1), 1–12.

Beck, M., Dellwig, L., Schnetger, B., Brumsack, H.J., 2008. Cycling of trace metals (Mn, Fe, Mo, U, V, Cr) in deep pore waters of intertidal flat sediments. Geochem. Cosmochim. Acta 72 (12), 2822–2840.

Beck, M., Reckhardt, A., Amelsberg, J., Bartholoma, A., Brumsack, H.J., Cypionka, H., Dittmar, T., Engelen, B., Greskowiak, J., Hillebrand, H., Holtappels, M., Neuholz, R., Koster, J., Kuypers, M.M.M., Massmann, G., Meier, D., Niggemann, J., Paffrath, R., Pahnke, K., Rovo, S., Striebel, M., Vandieken, V., Wehrmann, A., Zielinski, O., 2017. The drivers of biogeochemistry in beach ecosystems: a cross-shore transect from the dunes to the low-water line. Mar. Chem. 190, 35–50.

Blossier, B., Bryan, K.R., Daly, C.J., Winter, C., 2017. Spatial and temporal scales of shoreline morphodynamics derived from video camera observations for the island of Sylt, German Wadden Sea. Geo Mar. Lett. 37, 111–123. https://doi.org/10.1007/s00367-016-0461-7.

Blossier, B., Bryan, K.R., Daly, C.J., Winter, C., 2016. Nearshore sandbar rotation at single-barred embayed beaches. J. Geophys. Res.: Oceans 121, 2286–2313. https://doi.org/10.1002/2015JC011031.

Bratton, J.F., Bohlke, J.K., Manheim, F.T., Krantz, D.E., 2004. Ground water beneath coastal bays of the Delmarva peninsula: ages and nutrients. Ground Water 42 (7), 1021–1034.

Buquet, D., Sirieix, C., Anschutz, P., Malaurent, P., Charbonnier, C., Naessens, F., Bujan, S., Lecroart, P., 2016. Shape of the shallow aquifer at the fresh water-sea water interface on a high-energy sandy beach. Estuar. Coast Shelf Sci. 179, 79–89.

Cable, J.E., Martin, J.B., 2008. In situ evaluation of nearshore marine and fresh pore water transport into Flamengo Bay, Brazil. Estuar. Coast Shelf Sci. 76 (3), 473–483.

Cai, P.H., Wei, L., Geibert, W., Koehler, D., Ye, Y., Liu, W., Shi, X.M., 2020. Carbon and nutrient export from intertidal sand systems elucidated by $^{224}Ra/^{228}Th$ disequilibria. Geochem. Cosmochim. Acta 274, 302–316.

Calvache, M.L., Sánchez-Ubeda, J.P., Purtschert, R., López-Chicano, M., Martín-Montañés, C., Sültenfuss, J., Blanco-Coronas, A.M., Duque, C., 2020. Characterization of the functioning of the motril-salobrena coastal aquifer (SE Spain) through the use of environmental tracers. Environ. Earth Sci. 79 (6), 12.

Calvo-Martin, E., Alvarez-Salgado, X.A., Rocha, C., Ibánhez, J.S.P., 2021. Reactive Solute Transport Through Two Contrasting Subterranean Estuary Exit Sites in the Ilia de Vigo (NW Iberian Peninsula). Front. Mar. Sci. 8, 19.

Calvo-Martin, E., Teira, E., Alvarez-Salgado, X.A., Rocha, C., Jiang, S., Justel-Díez, M., Ibanhez, J.S.P., 2022. On the hidden diversity and niche specialization of the microbial realm of subterranean estuaries. Environ. Microbiol. 24 (12), 5859–5881.

Carmo, J.S.A., 2022. Dominant processes that amplify the swell towards the coast: the nazaré canyon and the giant waves. Res. Soc. Develop. 11 (11).

Castelle, B., Bonneton, P., Dupuis, H., Sénéchal, N., 2007. Double bar beach dynamics on the high-energy meso-macrotidal French Aquitanian Coast:: a review. Mar. Geol. 245 (1–4), 141–159.

Chaillou, G., Lemay-Borduas, F., Couturier, M., 2016. Transport and transformations of groundwater-borne carbon discharging through a sandy beach to a coastal ocean. Can. Water Resour. J. 41 (4), 455–468.

Chaillou, G., Lemay-Borduas, F., Larocque, M., Couturier, M., Biehler, A., Tommi-Morin, G., 2018. Flow and discharge of groundwater from a snowmelt-affected sandy beach. J. Hydrol. 557, 4–15.

Charbonnier, C., Anschutz, P., Abril, G., Mucci, A., Deirmendjian, L., Poirier, D., Bujan, S., Lecroart, P., 2022. Carbon dynamics driven by seawater recirculation and groundwater discharge along a forest-dune-beach continuum of a high-energy meso-macro-tidal sandy coast. Geochem. Cosmochim. Acta 317, 18–38.

Charbonnier, C., Anschutz, P., Deflandre, B., Bujan, S., Lecroart, P., 2016. Measuring pore water oxygen of a high-energy beach using buried probes. Estuar. Coast Shelf Sci. 179, 66–78.

Charbonnier, C., Anschutz, P., Poirier, D., Bujan, S., Lecroart, P., 2013. Aerobic respiration in a high-energy sandy beach. Mar. Chem. 155, 10–21.

Charette, M.A., Sholkovitz, E.R., 2002. Oxidative precipitation of groundwater-derived ferrous iron in the subterranean estuary of a coastal bay. Geophys. Res. Lett. 29 (10), 4.

Charette, M.A., Sholkovitz, E.R., 2006. Trace element cycling in a subterranean estuary: part 2. Geochemistry of the pore water. Geochem. Cosmochim. Acta 70 (4), 811–826.

Chen, X., Ye, Q., Sanders, C.J., Du, J., Zhang, J., 2020. Bacterial-derived nutrient and carbon source-sink behaviors in a sandy beach subterranean estuary. Mar. Pollut. Bull. 160, 111570.

Cheng, Y., Andersen, O.B., 2011. Multimission empirical ocean tide modeling for shallow waters and polar seas. J. Geophys. Res.: Oceans 116. https://doi.org/10.1029/2011JC007172.

Couturier, M., Nozais, C., Chaillou, G., 2016. Microtidal subterranean estuaries as a source of fresh terrestrial dissolved organic matter to the coastal ocean. Mar. Chem. 186, 46–57.

Couturier, M., Tommi-Morin, G., Sirois, M., Rao, A., Nozais, C., Chaillou, G., 2017. Nitrogen transformations along a shallow subterranean estuary. Biogeosciences 14 (13), 3321–3336.

Degenhardt, J., Dlugosch, L., Ahrens, J., Beck, M., Waska, H., Engelen, B., 2020. Seasonal dynamics of microbial diversity at a sandy high energy beach reveal a resilient core community. Front. Mar. Sci. 7.

Degenhardt, J., Khodami, S., Milke, F., Waska, H., Engelen, B., Arbizu, P.M., 2021a. The three domains of life within the discharge area of a shallow subterranean Estuary at a high energy beach. Front. Environ. Sci. 9, 15.

Degenhardt, J., Merder, J., Heyerhoff, B., Simon, H., Engelen, B., Waska, H., 2021b. Cross-Shore and depth zonations in bacterial diversity are linked to Age and source of dissolved organic matter across the intertidal area of a sandy beach. Microorganisms 9 (8).

Delgard, M.L., Deflandre, B., Metzger, E., Nuzzio, D., Capo, S., Mouret, A., Anschutz, P., 2012. In situ study of short-term variations of redox species chemistry in intertidal permeable sediments of the Arcachon lagoon. Hydrobiologia 699 (1), 69–84.

Dobrynin, M., Gayer, G., Pleskachevsky, A., Gunther, H., 2010. Effect of waves and currents on the dynamics and seasonal variations of suspended particulate matter in the north sea. J. Mar. Syst. 82 (1–2), 1–20.

Dugan, J.E., Hubbard, D.M., Page, H.M., Schimel, J.P., 2011. Marine macrophyte wrack inputs and dissolved nutrients in beach sands. Estuaries Coasts 34 (4), 839–850.

Dulaiova, H., Burnett, W.C., Chanton, J.P., Moore, W.S., Bokuniewicz, H.J., Charette, M. A., Sholkovitz, E., 2006. Assessment of groundwater discharges into west neck Bay, New York, via natural tracers. Cont. Shelf Res. 26 (16), 1971–1983.

Duque, C., Haider, K., Sebok, E., Sonnenborg, T.O., Engesgaard, P., 2018. A conceptual model for groundwater discharge to a coastal brackish lagoon based on seepage measurements (Ringkøbing Fjord, Denmark). Hydrol. Process. 32, 3352–3364. https://doi.org/10.1002/hyp.13264.

Duque, C., Michael, H.A., Wilson, A.M., 2020. The subterranean estuary: technical term, simple analogy, or source of confusion? Water Resour. Res. 56, e2019WR026554. https://doi.org/10.1029/2019WR026554.

Dyer, K., 1997. Estuaries: a Physical Introduction. Wiley, p. 195.

Ehlert, C., Reckhardt, A., Greskowiak, J., Liguori, B.T.P., Boning, P., Paffrath, R., Brumsack, H.J., Pahnke, K., 2016. Transformation of silicon in a sandy beach ecosystem: insights from stable silicon isotopes from fresh and saline groundwaters. Chem. Geol. 440, 207–218.

Erler, D.V., Santos, I.R., Zhang, Y., Tait, D.R., Befus, K.M., Hidden, A., Li, L., Eyre, B.D., 2014. Nitrogen transformations within a tropical subterranean estuary. Mar. Chem. 164, 38–47.

Evans, T.B., Wilson, A.M., 2016. Groundwater transport and the freshwater-saltwater interface below sandy beaches. J. Hydrol. 538, 563–573.

Evans, T.B., Wilson, A.M., 2017. Submarine groundwater discharge and solute transport under a transgressive barrier island. J. Hydrol. 547, 97–110.

Forehead, H., Thomson, P., Kendrick, G.A., 2013. Shifts in composition of microbial communities of subtidal sandy sediments maximise retention of nutrients. FEMS Microbiol. Ecol. 83 (2), 279–298.
Geng, X., Khalil, C.A., Prince, R.C., Lee, K., An, C., Boufadel, M.C., 2021a. Hypersaline pore water in Gulf of Mexico beaches prevented efficient biodegradation of deepwater horizon beached oil. Environ. Sci. Technol. 55 (20), 13792–13801.
Geng, X.L., Heiss, J.W., Michael, H.A., Li, H.L., Raubenheimer, B., Boufadel, M.C., 2021b. Geochemical fluxes in sandy beach aquifers: modulation due to major physical stressors, geologic heterogeneity, and nearshore morphology. Earth Sci. Rev. 221.
Gómez-Alvarez, P., Bates, B., Santos, I.R., Escobar Correa, R., Tucker, J.P., Ibrahim, N., Laicher-Edwards, D., Gardner, K., Silva Monteiro, L., Silva, D.A., Bowtell, J.R., Lin, H.A., Tolentino, N.L., Sanders, C.J., 2019. Submarine groundwater discharge revealed by ^{224}Ra and ^{223}Ra in coffs harbour, Australia. J. Radioanal. Nucl. Chem. 319 (3), 1193–1199.
Gonneea, M.E., Morris, P.J., Dulaiova, H., Charette, M.A., 2008. New perspectives on radium behavior within a subterranean estuary. Mar. Chem. 109 (3–4), 250–267.
Gonneea, M.E., Mulligan, A.E., Charette, M.A., 2013. Seasonal cycles in radium and barium within a subterranean estuary: implications for groundwater derived chemical fluxes to surface waters. Geochem. Cosmochim. Acta 119, 164–177.
Goodridge, B.M., 2018. The influence of submarine groundwater discharge on nearshore marine dissolved organic carbon reactivity, concentration dynamics, and offshore export. Geochem. Cosmochim. Acta 241, 108–119.
Goodridge, B.M., Melack, J.M., 2014. Temporal evolution and variability of dissolved inorganic nitrogen in beach pore water revealed using radon residence times. Environ. Sci. Technol. 48 (24), 14211–14218.
Greskowiak, J., 2014. Tide-induced salt-fingering flow during submarine groundwater discharge. Geophys. Res. Lett. 41 (18), 6413–6419.
Greskowiak, J., Massmann, G., 2021. The impact of morphodynamics and storm floods on pore water flow and transport in the subterranean estuary. Hydrol. Process. 35 (3), 5.
Greskowiak, J., Seibert, S.L., Post, V.E.A., Massmann, G., 2023. Redox-zoning in high-energy subterranean estuaries as a function of storm floods, temperatures, seasonal groundwater recharge and morphodynamics. Estuar. Coast Shelf Sci. 290, 11.
Grünenbaum, N., Ahrens, J., Beck, M., Gilfedder, B.S., Greskowiak, J., Kossack, M., Massmann, G., 2020a. A multi-method approach for quantification of In- and exfiltration rates from the subterranean Estuary of a high energy beach. Front. Earth Sci. 8, 15.
Grünenbaum, N., Greskowiak, J., Sultenfuss, J., Massmann, G., 2020b. Groundwater flow and residence times below a meso-tidal high-energy beach: a model-based analyses of salinity patterns and H-3-He-3 groundwater ages. J. Hydrol. 587, 12.
Grünenbaum, N., Günther, T., Greskowiak, J., Vienken, T., Müller-Petke, M., Massmann, G., 2023. Salinity distribution in the subterranean estuary of a meso-tidal high-energy beach characterized by electrical resistivity tomography and direct push technology. J. Hydrol. 617, 10.
Grünenbaum, N., Volk, V., Delwar, R.B., Bräunig, L., Massmann, G., Greskowiak, J., 2024. Visualizing the 'iron curtain' formation in the subterranean estuary using sand tank experiments. Hydrol. Process. 38, e15129.
Hayes, M.O., 1979. Barrier island morphology as a function of tidal and wave regime. In: Leatherman, S.P. (Ed.), Barrier Islands. Academic Press, New York.
Heiss, J.W., Michael, H.A., 2014. Saltwater-freshwater mixing dynamics in a sandy beach aquifer over tidal, spring-neap, and seasonal cycles. Water Resour. Res. 50 (8), 6747–6766.
Heiss, J.W., Ullman, W.J., Michael, H.A., 2014. Swash zone moisture dynamics and unsaturated infiltration in two sandy beach aquifers. Estuar. Coast Shelf Sci. 143, 20–31.
Herrling, G., Winter, C., 2017. Spatiotemporal variability of sedimentology and morphology in the East Frisian barrier island system. Geo Mar. Lett. 37 (2), 137–149.
Herrling, G., Winter, C., 2018. Tidal inlet sediment bypassing at mixed-energy barrier islands. Coast. Eng. 140, 342–354.
Howarth, R.W., Marino, R., 2006. Nitrogen as the limiting nutrient for eutrophication in coastal marine ecosystems: evolving views over three decades. Limnol. Oceanogr. 51 (1), 364–376.
Hwang, D.W., Kim, G.B., Lee, Y.W., Yang, H.S., 2005. Estimating submarine inputs of groundwater and nutrients to a coastal bay using radium isotopes. Mar. Chem. 96 (1–2), 61–71.
Ibánhez, J.S.P., Rocha, C., 2016. Oxygen transport and reactivity within a sandy seepage face in a mesotidal lagoon (Ria Formosa, Southwestern Iberia). Limnol. Oceanogr. 61 (1), 61–77.
Johannesson, K.H., Chevis, D.A., Burdige, D.J., Cable, J.E., Martin, J.B., Roy, M., 2011. Submarine groundwater discharge is an important net source of light and middle REEs to coastal waters of the Indian River Lagoon, Florida, USA. Geochem. Cosmochim. Acta 75 (3), 825–843.
Kim, K.H., Heiss, J.W., Geng, X., Michael, H.A., 2020. Modeling hydrologic controls on particulate organic carbon contributions to beach aquifer biogeochemical reactivity. Water Resour. Res. 56 (10), e2020WR027306.
Kim, K.H., Heiss, J.W., Michael, H.A., Cai, W.J., Laattoe, T., Post, V.E.A., Ullman, W.J., 2017. Spatial patterns of groundwater biogeochemical reactivity in an intertidal beach aquifer. J. Geophys. Res. Biogeosci. 122 (10), 2548–2562.
Kim, K.H., Heiss, J.W., Michael, H.A., Ullman, W.J., Cai, W.J., 2022. Seasonal and spatial production patterns of dissolved inorganic carbon and total alkalinity in a shallow beach aquifer. Front. Mar. Sci. 9, 12.
Kroeger, K.D., Charette, M.A., 2008. Nitrogen biogeochemistry of submarine groundwater discharge. Limnol. Oceanogr. 53 (3), 1025–1039.
Kroeger, K.D., Swarzenski, P.W., Greenwood, W.J., Reich, C., 2007. Submarine groundwater discharge to Tampa Bay: nutrient fluxes and biogeochemistry of the coastal aquifer. Mar. Chem. 104 (1–2), 85–97.
Lecher, A.L., Chien, C.T., Paytan, A., 2016. Submarine groundwater discharge as a source of nutrients to the north Pacific and arctic coastal ocean. Mar. Chem. 186, 167–177.
Lettmann, K.A., Wolff, J.O., Badewien, T.H., 2009. Modeling the impact of wind and waves on suspended particulate matter fluxes in the East Frisian Wadden Sea (southern North Sea). Ocean Dyn. 59 (2), 239–262.
Li, H.L., Boufadel, M.C., 2010. Long-term persistence of oil from the *Exxon Valdez* spill in two-layer beaches. Nat. Geosci. 3 (2), 96–99.
Li, X.Y., Hu, B.X., Burnett, W.C., Santos, I.R., Chanton, J.P., 2009. Submarine ground water discharge driven by tidal pumping in a heterogeneous aquifer. Ground Water 47 (4), 558–568.
Linkhorst, A., Dittmar, T., Waska, H., 2017. Molecular fractionation of dissolved organic matter in a shallow subterranean Estuary: the role of the iron curtain. Environ. Sci. Technol. 51 (3), 1312–1320.
Liu, Q., Charette, M.A., Breier, C.F., Henderson, P.B., McCorkle, D.C., Martin, W., Dai, M. H., 2017. Carbonate system biogeochemistry in a subterranean estuary - Waquoit Bay, USA. Geochem. Cosmochim. Acta 203, 422–439.
Liu, Y., Jiao, J.J., Liang, W.Z., 2018a. Tidal fluctuation influenced physicochemical parameter dynamics in coastal groundwater mixing Zone. Estuaries Coasts 41 (4), 988–1001.
Liu, Y., Liang, W.Z., Jiao, J.J., 2018b. Seasonality of nutrient flux and biogeochemistry in an intertidal aquifer. J. Geophys. Res. Oceans 123 (9), 6116–6135.
Loveless, A.M., Oldham, C.E., 2010. Natural attenuation of nitrogen in groundwater discharging through a sandy beach. Biogeochemistry 98 (1–3), 75–87.
Loveless, A.M., Oldham, C.E., Hancock, G.J., 2008. Radium isotopes reveal seasonal groundwater inputs to cockburn sound, a marine embayment in Western Australia. J. Hydrol. 351 (1–2), 203–217.
Luijendijk, A., Hagenaars, G., Ranasinghe, R., Baart, F., Donchyts, G., Aarninkhof, S., 2018. The state of the World's beaches (vol 8, 6641, 2018). Sci. Rep. 8, 1.
Luijendijk, E., Gleeson, T., Moosdorf, N., 2020. Fresh groundwater discharge insignificant for the world's oceans but important for coastal ecosystems. Nat. Commun. 11, 1260. https://doi.org/10.1038/s41467-020-15064-8.
Martínez-Pérez, L., Luquot, L., Carrera, J., Marazuela, M.A., Goyetche, T., Pool, M., Palacios, A., Bellmunt, F., Ledo, J., Ferrer, N., del Val, L., Pezard, P.A., García-Orellana, J., Diego-Feliu, M., Rodellas, V., Saaltink, M.W., Vázquez-Suñé, E., Folch, A., 2022. A multidisciplinary approach to characterizing coastal alluvial aquifers to improve understanding of seawater intrusion and submarine groundwater discharge. J. Hydrol. 607, 18.
Massmann, G., Abarike, G., Amoako, K., Auer, F., Badewien, T.H., Berkenbrink, C., Böttcher, M.E., Brick, S., Cordova, I.V.M., Cueto, J., Dittmar, T., Engelen, B., Freund, H., Greskowiak, J., Guenther, T., Herbst, G., Holtappels, M., Marchant, H.K., Meyer, R., Müller-Petke, M., Niggemann, J., Pahnke, K., Pommerin, D., Post, V., Reckhardt, A., Roberts, M., Schwalfenberg, K., Seibert, S.L., Siebert, C., Skibbe, N., Waska, H., Winter, C., Zielinski, O., 2023. The DynaDeep observatory - a unique approach to study high-energy subterranean estuaries. Front. Mar. Sci. 10, 24.
McAllister, S.M., Barnett, J.M., Heiss, J.W., Findlay, A.J., MacDonald, D.J., Dow, C.L., Luther, G.W., Michael, H.A., Chan, C.S., 2015. Dynamic hydrologic and biogeochemical processes drive microbially enhanced iron and sulfur cycling within the intertidal mixing zone of a beach aquifer. Limnol. Oceanogr. 60 (1), 329–345.
McBeth, J.M., Fleming, E.J., Emerson, D., 2013. The transition from freshwater to marine iron-oxidizing bacterial lineages along a salinity gradient on the sheepscot river, Maine, USA. Environ. Microbiol. Rep. 5 (3), 453–463.
McLachlan, A., Defeo, O., 2018. The Ecology of Sandy Shores. Elsevier.
McLachlan, A., Defeo, O., Short, A.D., 2018. Characterising sandy beaches into major types and states: implications for ecologists and managers. Estuar. Coast Shelf Sci. 215, 152–160.
McLachlan, A., Turner, I., 1994. The Interstidal environment of sandy beaches. Marine Ecol. Pubblicazioni Della Stazione Zoologica Di Napoli I 15 (3–4), 177–211.
Michael, H.A., Mulligan, A.E., Harvey, C.F., 2005. Seasonal oscillations in water exchange between aquifers and the coastal ocean. Nature 436 (7054), 1145–1148.
Michael, H.A., Post, V.E.A., Wilson, A.M., Werner, A.D., 2017. Science, society, and the coastal groundwater squeeze. Water Resour. Res. 53 (4), 2610–2617.
Moore, W.S., 1999. The subterranean estuary: a reaction zone of ground water and sea water. Mar. Chem. 65 (1–2), 111–125.
Moore, W.S., 2010. The effect of submarine groundwater discharge on the Ocean. Ann. Rev. Mar. Sci 2, 59–88.
Moore, W.S., Humphries, M.S., Benitez-Nelson, C.R., Pillay, L., Higgs, C., 2019. Transport of radium and nutrients through eastern South African beaches. J. Geophys. Res. Oceans 124 (3), 2010–2027.
Moosdorf, N., Bottcher, M.E., Adyasari, D., Erkul, E., Gilfedder, B.S., Greskowiak, J., Jenner, A.K., Kotwicki, L., Massmann, G., Muller-Petke, M., Oehler, T., Post, V., Prien, R., Scholten, J., Siemon, B., von Ahn, C.M.E., Walther, M., Waska, H., Wunderlich, T., Mallast, U., 2021. A state-of-the-art perspective on the characterization of subterranean estuaries at the regional scale. Front. Earth Sci. 9, 26.
Moosdorf, N., Tschaikowski, J., Kretschmer, D., Reinecke, R., 2024. A global coastal permeability dataset (CoPerm 1.0). Sci. Data 11, 893. https://doi.org/10.1038/s41597-024-03749-4.
Mulhern, J.S., Johnson, C.L., Martin, J.M., 2017. Is barrier island morphology a function of tidal and wave regime? Mar. Geol. 387, 74–84.
Mulligan, A.E., Langevin, C., Post, V.E.A., 2011. Tidal boundary conditions in SEAWAT. Ground Water 49 (6), 866–879.
Nel, R., Campbell, E.E., Harris, L., Hauser, L., Schoeman, D.S., McLachlan, A., du Preez, D.R., Bezuidenhout, K., Schlacher, T.A., 2014. The status of sandy beach science: past trends, progress, and possible futures. Estuar. Coast Shelf Sci. 150, 1–10.

Null, K.A., Corbett, D.R., DeMaster, D.J., Burkholder, J.M., Thomas, C.J., Reed, R.E., 2011. Porewater advection of ammonium into the neuse river Estuary, North Carolina, USA. Estuar. Coast Shelf Sci. 95 (2–3), 314–325.
O'Connor, A.E., Canuel, E.A., Beck, A.J., 2022. Drivers and seasonal variability of redox-sensitive metal chemistry in a shallow subterranean Estuary. Front. Environ. Sci. 9, 17.
O'Connor, A.E., Krask, J.L., Canuel, E.A., Beck, A.J., 2018. Seasonality of major redox constituents in a shallow subterranean estuary. Geochem. Cosmochim. Acta 224, 344–361.
O'Connor, A.E., Luek, J.L., McIntosh, H., Beck, A.J., 2015. Geochemistry of redox-sensitive trace elements in a shallow subterranean estuary. Mar. Chem. 172, 70–81.
Oehler, T., Ramasamy, M., George, M.E., Babu, S.D.S., Daehnke, K., Ankele, M., Boettcher, M.E., Santos, I.R., Moosdorf, N., 2021. Tropical beaches attenuate groundwater nitrogen pollution flowing to the ocean. Environ. Sci. Technol. 55 (12), 8432–8438.
Paffrath, R., Pahnke, K., Behrens, M.K., Reckhardt, A., Ehlert, C., Schnetger, B., Brumsack, H.J., 2020. Rare Earth element behavior in a sandy subterranean Estuary of the southern north sea. Front. Mar. Sci. 7, 18.
Pit, I.R., Griffioen, J., Wassen, M.J., 2017. Environmental geochemistry of a mega beach nourishment in the Netherlands: monitoring freshening and oxidation processes. Appl. Geochem. 80, 72–89.
Poppe, L.J., Moffett, A.M., 1993. Ground-water discharge and related nutrient andand trace metal fluxes into Quincy Bay, Massachusetts. Environ. Monit. Assess. 25 (1), 15–27.
Prakash, R., Loveson, V.J., Kessarkar, P.M., Kumar, A., Pesso, C., Gomes, C., 2024. Fresh and recirculated submarine groundwater discharge zones along the central west coast of India. Environ. Res. 250, 14.
Qu, W., Li, H., Huang, H., Zheng, C., Wang, C., Wang, X., Zhang, Y., 2017. Seawater-groundwater exchange and nutrients carried by submarine groundwater discharge in different types of wetlands at Jiaozhou Bay, China. J. Hydrol. 555, 185–197.
Reckhardt, A., Beck, M., Greskowiak, J., Schnetger, B., Bottcher, M.E., Gehre, M., Brumsack, H.J., 2017. Cycling of redox-sensitive elements in a sandy subterranean estuary of the southern north sea. Mar. Chem. 188, 6–17.
Reckhardt, A., Beck, M., Seidel, M., Riedel, T., Wehrmann, A., Bartholoma, A., Schnetger, B., Dittmar, T., Brumsack, H.J., 2015. Carbon, nutrient and trace metal cycling in sandy sediments: a comparison of high-energy beaches and backbarrier tidal flats. Estuar. Coast Shelf Sci. 159, 1–14.
Robinson, C., Gibbes, B., Carey, H., Li, L., 2007a. Salt-freshwater dynamics in a subterranean estuary over a spring-neap tidal cycle. J. Geophys. Res. Oceans 112 (C9), 15.
Robinson, C., Gibbes, B., Li, L., 2006. Driving mechanisms for groundwater flow and salt transport in a subterranean estuary. Geophys. Res. Lett. 33 (3), 4.
Robinson, C., Li, L., Barry, D.A., 2007b. Effect of tidal forcing on a subterranean estuary. Adv. Water Resour. 30 (4), 851–865.
Robinson, C., Xin, P., Li, L., Barry, D.A., 2014. Groundwater flow and salt transport in a subterranean estuary driven by intensified wave conditions. Water Resour. Res. 50 (1), 165–181.
Robinson, C.E., Xin, P., Santos, I.R., Charette, M.A., Li, L., Barry, D.A., 2018. Groundwater dynamics in subterranean estuaries of coastal unconfined aquifers: controls on submarine groundwater discharge and chemical inputs to the ocean. Adv. Water Resour. 115, 315–331.
Robinson, M., Gallagher, D., Reay, W., 1998. Field observations of tidal and seasonal variations in ground water discharge to tidal estuarine surface water. Ground Water Monit. Remed. 18 (1), 83–92.
Rodellas, V., Garcia-Orellana, J., Masque, P., Feldman, M., Weinstein, Y., 2015. Submarine groundwater discharge as a major source of nutrients to the Mediterranean Sea. Proc. Natl. Acad. Sci. U. S. A 112 (13), 3926–3930.
Rodellas, V., Garcia-Orellana, J., Trezzi, G., Masque, P., Stieglitz, T.C., Bokuniewicz, H., Cochran, J.K., Berdalet, E., 2017. Using the radium quartet to quantify submarine groundwater discharge and porewater exchange. Geochem. Cosmochim. Acta 196, 58–73.
Roper, T., Greskowiak, J., Massmann, G., 2015. Instabilities of submarine groundwater discharge under tidal forcing. Limnol. Oceanogr. 60 (1), 22–28.
Roper, T., Kroger, K.F., Meyer, H., Sultenfuss, J., Greskowiak, J., Massmann, G., 2012. Groundwater ages, recharge conditions and hydrochemical evolution of a barrier island freshwater lens (Spiekeroog, Northern Germany). J. Hydrol. 454, 173–186.
Roy, M., Rouxel, O., Martin, J.B., Cable, J.E., 2012. Iron isotope fractionation in a sulfide-bearing subterranean estuary and its potential influence on oceanic Fe isotope flux. Chem. Geol. 300, 133–142.
Ruiz-González, C., Rodríguez-Pie, L., Maister, O., Rodellas, V., Alorda-Keinglass, A., Diego-Feliu, M., Folch, A., Garcia-Orellana, J., Gasol, J.M., 2022. High spatial heterogeneity and low connectivity of bacterial communities along a Mediterranean subterranean estuary. Mol. Ecol. 31 (22), 5745–5764.
Sáenz, J.P., Hopmans, E.C., Rogers, D., Henderson, P.B., Charette, M.A., Schouten, S., Casciotti, K.L., Sinninghe Damsté, J.S., Eglinton, T.I., 2012. Distribution of anaerobic ammonia-oxidizing bacteria in a subterranean estuary. Mar. Chem. 136–137, 7–13. https://doi.org/10.1016/j.marchem.2012.04.004.
Sanders, C.J., Santos, I.R., Sadat-Noori, M., Maher, D.T., Holloway, C., Schnetger, B., Brumsack, H.J., 2017. Uranium export from a sandy beach subterranean estuary in Australia. Estuar. Coast Shelf Sci. 198, 204–212.
Santos, I.R., Burnett, W.C., Chanton, J., Mwashote, B., Suryaputra, I., Dittmar, T., 2008. Nutrient biogeochemistry in a Gulf of Mexico subterranean estuary and groundwater-derived fluxes to the coastal ocean. Limnol. Oceanogr. 53 (2), 705–718.
Santos, I.R., Burnett, W.C., Dittmar, T., Suryaputra, I.G.N.A., Chanton, J., 2009. Tidal pumping drives nutrient and dissolved organic matter dynamics in a Gulf of Mexico subterranean estuary. Geochem. Cosmochim. Acta 73 (5), 1325–1339.
Santos, I.R., Burnett, W.C., Misra, S., Suryaputra, I., Chanton, J.P., Dittmar, T., Peterson, R.N., Swarzenski, P.W., 2011. Uranium and barium cycling in a salt wedge subterranean estuary: the influence of tidal pumping. Chem. Geol. 287 (1–2), 114–123.
Santos, I.R., Eyre, B.D., Huettel, M., 2012. The driving forces of porewater and groundwater flow in permeable coastal sediments: a review. Estuar. Coast Shelf Sci. 98, 1–15.
Sawyer, A.H., David, C.H., Famiglietti, J.S., 2016. Continental patterns of submarine groundwater discharge reveal coastal vulnerabilities. Science 353 (6300), 705–707.
Seibert, S.L., Böttcher, M.E., Schubert, F., Pollmann, T., Giani, L., Tsukamoto, S., Frechen, M., Freund, H., Waska, H., Simon, H., Holt, T., Greskowiak, J., Massmann, G., 2019. Iron sulfide formation in young and rapidly-deposited permeable sands at the land-sea transition zone. Sci. Total Environ. 649, 264–283. https://doi.org/10.1016/j.scitotenv.2018.08.278.
Shen, C.J., Zhang, C.M., Kong, J., Xin, P., Lu, C.H., Zhao, Z.W., Li, L., 2019. Solute transport influenced by unstable flow in beach aquifers. Adv. Water Resour. 125, 68–81.
Sirois, M., Couturier, M., Barber, A., Gélinas, Y., Chaillou, G., 2018. Interactions between iron and organic carbon in a sandy beach subterranean estuary. Mar. Chem. 202, 86–96.
Snyder, M., Taillefert, M., Ruppel, C., 2004. Redox zonation at the saline-influenced boundaries of a permeable surficial aquifer: effects of physical forcing on the biogeochemical cycling of iron and manganese. J. Hydrol. 296 (1), 164–178.
Spiteri, C., Slomp, C.P., Charette, M.A., Tuncay, K., Meile, C., 2008. Flow and nutrient dynamics in a subterranean estuary (Waquoit Bay, MA, USA): field data and reactive transport modeling. Geochem. Cosmochim. Acta 72 (14), 3398–3412.
Swarzenski, P.W., Izbicki, J.A., 2009. Coastal groundwater dynamics off Santa Barbara, California: combining geochemical tracers, electromagnetic seepmeters, and electrical resistivity. Estuar. Coast Shelf Sci. 83 (1), 77–89.
Talbot, J.M., Kroeger, K.D., Rago, A., Allen, M.C., Charette, M.A., 2003. Nitrogen flux and speciation through the subterranean estuary of Waquoit Bay, Massachusetts. Biol. Bull. 205 (2), 244–245.
Tamborski, J.J., Cochran, J.K., Bokuniewicz, H.J., 2017. Application of ^{224}Ra and ^{222}Rn for evaluating seawater residence times in a tidal subterranean estuary. Mar. Chem. 189, 32–45.
Taniguchi, M., Turner, J.V., Smith, A.J., 2003. Evaluations of groundwater discharge rates from subsurface temperature in cockburn sound, Western Australia. Biogeochemistry 66 (1–2), 111–124.
Toro, M., Ptak, T., Massmann, G., SultenfuB, J., Janssen, M., 2022. Groundwater flow patterns in a coastal fen exposed to drainage, rewetting and interaction with the Baltic sea. J. Hydrol. 615, 12.
Tyler, P., Amaro, T., Arzola, R., Cunha, M.R., de Stigter, H., Gooday, A., Huvenne, V., Ingels, J., Kiriakoulakis, K., Lastras, G., Masson, D., Oliveira, A., Pattenden, A., Vanreusel, A., Van Weering, T., Vitorino, J., Witte, U., Wolff, G., 2009. Europe's grand canyon nazare submarine canyon. Oceanography (Wash. D. C.) 22 (1), 46–57.
Ullman, W.J., Chang, B., Miller, D.C., Madsen, J.A., 2003. Groundwater mixing, nutrient diagenesis, and discharges across a sandy beachface, cape henlopen, Delaware (USA). Estuar. Coast Shelf Sci. 57 (3), 539–552.
Urish, D.W., McKenna, T.E., 2004. Tidal effects on ground water discharge through a sandy marine beach. Ground Water 42 (7), 971–982.
Wang, Z.Y., Wang, Q.Q., Guo, Y.F., Yu, S.C., Xiao, K., Zhang, Y., Li, H.L., Zheng, C.M., Geng, X.L., Zhang, X.L., Li, H.J., Wang, X.J., 2023. Seawater-groundwater interaction governs trace metal zonation in a coastal sandy aquifer. Water Resour. Res. 59 (9), 21.
Waska, H., Brumsack, H.J., Massmann, G., Koschinsky, A., Schnetger, B., Simon, H., Dittmar, T., 2019a. Inorganic and organic iron and copper species of the subterranean estuary: origins and fate. Geochem. Cosmochim. Acta 259, 211–232.
Waska, H., Greskowiak, J., Ahrens, J., Beck, M., Ahmerkamp, S., Boning, P., Brumsack, H.J., Degenhardt, J., Ehlert, C., Engelen, B., Grünenbaum, N., Holtappels, M., Pahnke, K., Marchant, H.K., Massmann, G., Meier, D., Schnetger, B., Schwalfenberg, K., Simon, H., Vandieken, V., Zielinski, O., Dittmar, T., 2019b. Spatial and temporal patterns of pore water chemistry in the inter-tidal Zone of a high energy beach. Front. Mar. Sci. 6, 16.
Waska, H., Simon, H., Ahmerkamp, S., Greskowiak, J., Ahrens, J., Seibert, S.L., Schwalfenberg, K., Zielinski, O., Dittmar, T., 2021. Molecular traits of dissolved organic matter in the subterranean Estuary of a high-energy beach: indications of sources and sinks. Front. Mar. Sci. 8.
WAVEWATCH III R© Development Group (WW3DG), 2019. User Manual and System Documentation of WAVEWATCH II R© Version 6.07. Tech. Note, vol. 333. NOAA/NWS/NCEP/MMAB, College Park, MD, USA, p. 465. + Appendices.
Wilson, S.J., Anderson, I.C., Song, B.K., Tobias, C.R., 2023. Temporal and spatial variations in subterranean Estuary geochemical gradients and nutrient cycling rates: impacts on groundwater nutrient export to estuaries. J. Geophys. Res. Biogeosci. 128 (6), 19.
Wilson, S.J., Moody, A., McKenzie, T., Cardenas, M.B., Luijendijk, E., Sawyer, A.H., Wilson, A., Michael, H.A., Xu, B., Knee, K.L., Cho, H.-M., Weinstein, Y., Paytan, A., Moosdorf, N., Chen, C.-T.A., Beck, M., Lopez, C., Murgulet, D., Kim, G., Charette, M. A., Waska, H., Ibánhez, J.S.P., Chaillou, G., Oehler, T., Onodera, S.-i., Saito, M., Rodellas, V., Dimova, N., Montiel, D., Dulai, H., Richardson, C., Du, J., Petermann, E., Chen, X., Davis, K.L., Lamontagne, S., Sugimoto, R., Wang, G., Li, H., Torres, A.I., Demir, C., Bristol, E., Connolly, C.T., McClelland, J.W., Silva, B.J., Tait, D., Kumar, B., Viswanadham, R., Sarma, V., Silva-Filho, E., Shiller, A., Lecher, A., Tamborski, J., Bokuniewicz, H., Rocha, C., Reckhardt, A., Böttcher, M.E.,

Jiang, S., Stieglitz, T., Gbewezoun, H.G.V., Charbonnier, C., Anschutz, P., Hernández-Terrones, L.M., Babu, S., Szymczycha, B., Sadat-Noori, M., Niencheski, F., Null, K., Tobias, C., Song, B., Anderson, I.C., Santos, I.R., 2024. Global subterranean estuaries modify groundwater nutrient loading to the ocean. Limnol. Oceanogr. Lett. 9, 411–422.

Zhang, Y., Guo, Y.F., Wang, J.J., Maher, D.T., Geng, X.L., Wang, Q.Q., Xiao, K., Ding, H., Li, H.L., Zheng, C.M., Wang, Z.Y., Wang, X.J., 2024. Dissolved carbon dynamics and exchange in a high permeability beach aquifer. Geochem. Cosmochim. Acta 368, 64–75.

Zhang, Y.F., Wu, J.X., Zhang, K.K., Guo, X.J., Xing, C., Li, N., Wu, H.F., 2021. Analysis of seasonal differences in tidally influenced groundwater discharge processes in sandy tidal flats: a case study of Shilaoren Beach, Qingdao, China. J. Hydrol. 603, 14.

Zamrsky, D., Oude Essink, G.H.P., Bierkens, M.F.P., 2018. Estimating the thickness of unconsolidated coastal aquifers along the global coastline. Earth Syst. Sci. Data 10, 1591–1603. https://doi.org/10.5194/essd-10-1591-2018.